Experience with Testing and Application of Cable-in-Conduit Conductors (CICC)

Friday, September 24, 1993
Victoria, B.C.

Development of Forced-Flow Cooled Superconducting Poloidal Coils for Large Helical Device

Toshiyuki Mito

National Institute for Fusion Science (NIFS)
Toki 509-52, Japan

Contents:

- Research works in NIFS to construct poloidal field coils for Large Helical Device (LHD) are reviewed.
- Our experiences are restricted to a NbTi cable-in-conduit conductor. However a NbTi coil has simple superconducting characteristics compared with a Nb_3Sn coil. It is suitable for understanding fundamental characteristics of CICC.

Focus:

- Relation between Current Distribution and Stability
- Optimization of Stability and AC Loss

Items

1. Poloidal Coils for Large Helical Device

2. R&D of Forced-Flow Cooled Coils
   with a NbTi CICC

   2-1 Development and Test of TOKI-PF Coil
   2-2 Test of IV-S Coil with an Improved Conductor
   2-3 Short Sample Tests of IV Conductor
   Measurements of Current Distribution with Pick-Up Coils
   2-4 Measurements of AC losses

3. Future R&D Plan

4. Summary

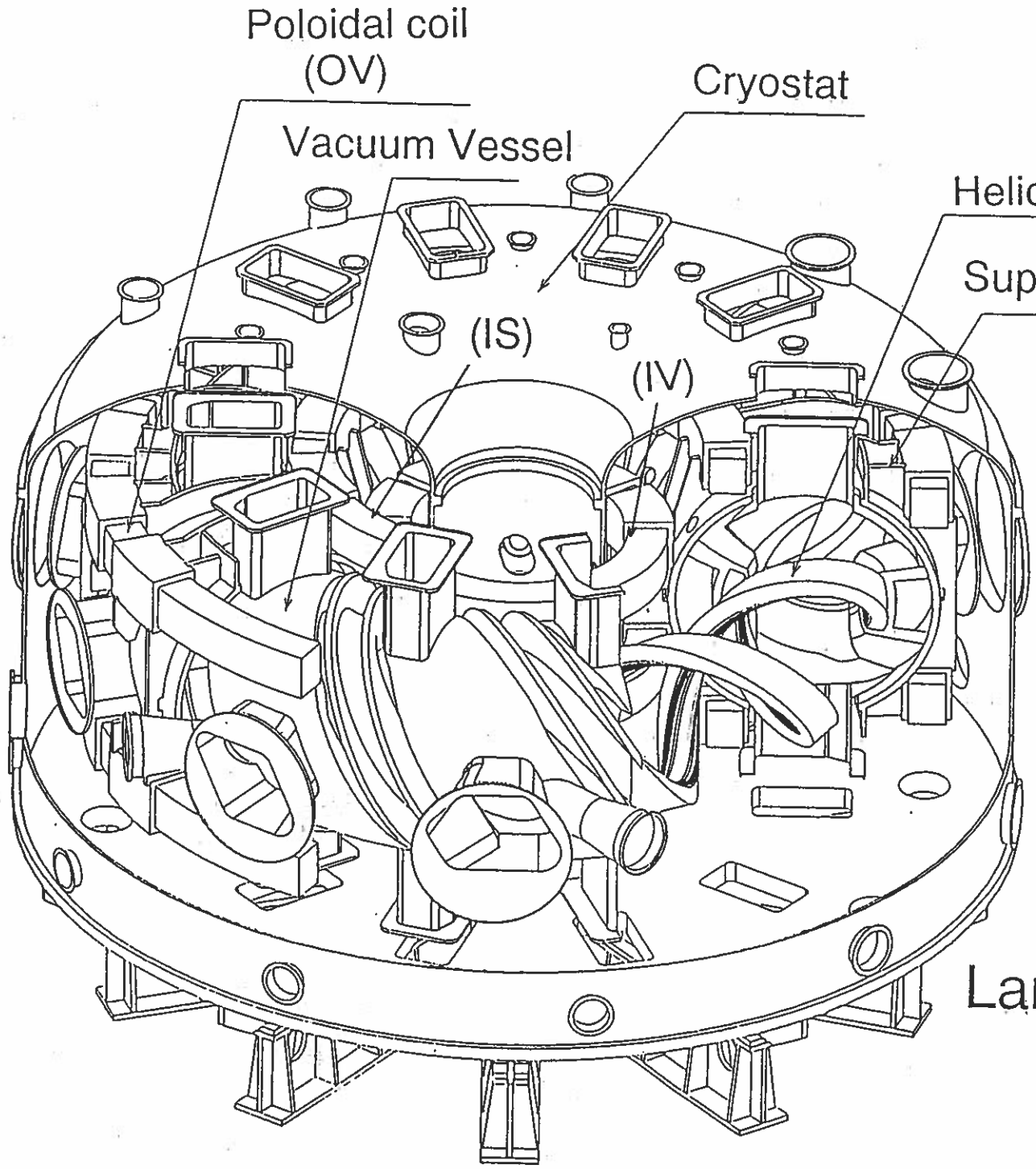

Large Helical Device
LHD

LHD

Large ***H***elical ***D***evice (LHD) is a heliotron type fusion experimental device.

The construction of LHD was started in 1991 and will be completed in 1996.

One of the main feature of LHD is to use superconducting coils as all coils for magnetic confinement (two helical coils and three pairs of poloidal coils).

Major radius:	3.9	m
Minor radius:	0.975	m
Central magnetic field:	3 T (in phase I) 4 T (in phase II)	

Specifications of LHD poloidal coils

	UNIT	OV COIL	IS COIL	IV COIL
AVERAGE RADIUS	mm	5650	2820	1800
CENTER POSITION	mm	+-1550	+-2000	+-800
MAGNETMOTIV FORCE	MAT	-4.5	-4.5	5.0
COIL CURRENT	kA	-31.3	-21.6	20.8
NUMBER OF TURNS		9X16	13X16	15X16
		=144	=208	=240
MAXIMUM FIELD	T	5.0	5.4	6.5
INDUCTANCE	H	0.514	0.445	0.313
CONDUCTOR SIZE	mmXmm	30.5X30.5	23X27.6	23X27.6
COIL SIZE	mmXmm	291.5X519.5	320X473.1	368X473.1
CURRENT DENSITY	A/mm2	-31.0	-31.0	29.8
CONDUCTOR LENGTH	m	5022	3685	2714
LENGTH OF FLOW PATH	m	314	230	170
NUMBER OF FLOW PATH		16	16	16
SHE MASS FLOW RATE	g/s	80	66	80

Poloidal Field Coils of LHD

Three pairs of poloidal coils are designed as forced-flow cooled superconducting coils with a NbTi cable-in conduit conductor.

These poloidal coils are operated in constant current at phase I.

Constant current operation is a main operational mode of the poloidal coils.

Pulse operation of poloidal coils (Its changing time duration is 5 seconds and the time interval is 5 minutes) is planned as one of the variety of plasma physics experiments in phase II.

Therefore the design of the poloidal coils have been done making importance on the stability in constant current operation.

2. R&D of Forced-Flow Cooled Coils with a NbTi CICC

2-1 Development and Test of TOKI-PF Coil

2-2 Test of IV-S Coil with an Improved Conductor

2-3 Short Sample Tests of IV Conductor

Measurements of Current Distribution with Pick-Up Coils

2-4 Measurements of AC losses

Principal specifications of the TOKI-PF coil

Conductor		Coil	
Type	Cable-in-conduit	Configuration	Two double pancakes
Superconducting material	NbTi	Inner radius	0.6 m
Critical current	50 kA at 7 T	Outer radius	0.82 m
Conduit dimension	17.0 × 22.5 mm	Height	0.11 m
Void fraction	0.4	Operating current	25.6 kA at 2.76 T
Strand diameter	0.67 mm with formvar (10 μm)	Number of turns	40
Number of strands	486	Inductance	3.18 mH
NbTi : Cu : CuNi	1.0 : 1.6 : 0.5	Stored energy	1.04 MJ

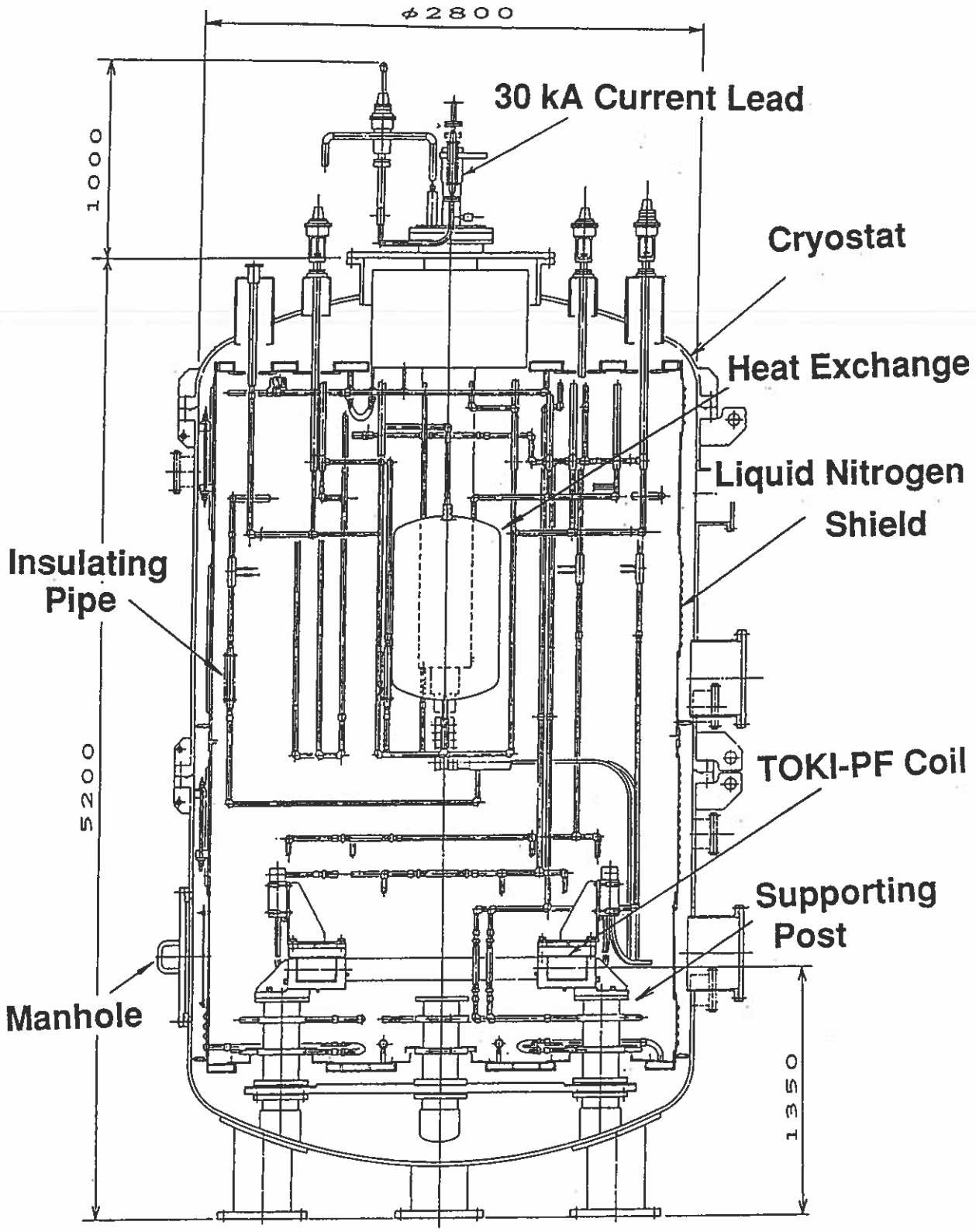
φ2800
1000
30 kA Current Lead
Cryostat
Heat Exchange
Liquid Nitrogen
Shield
Insulating
Pipe
5200
TOKI-PF Coil
Supporting
Post
Manhole
1350

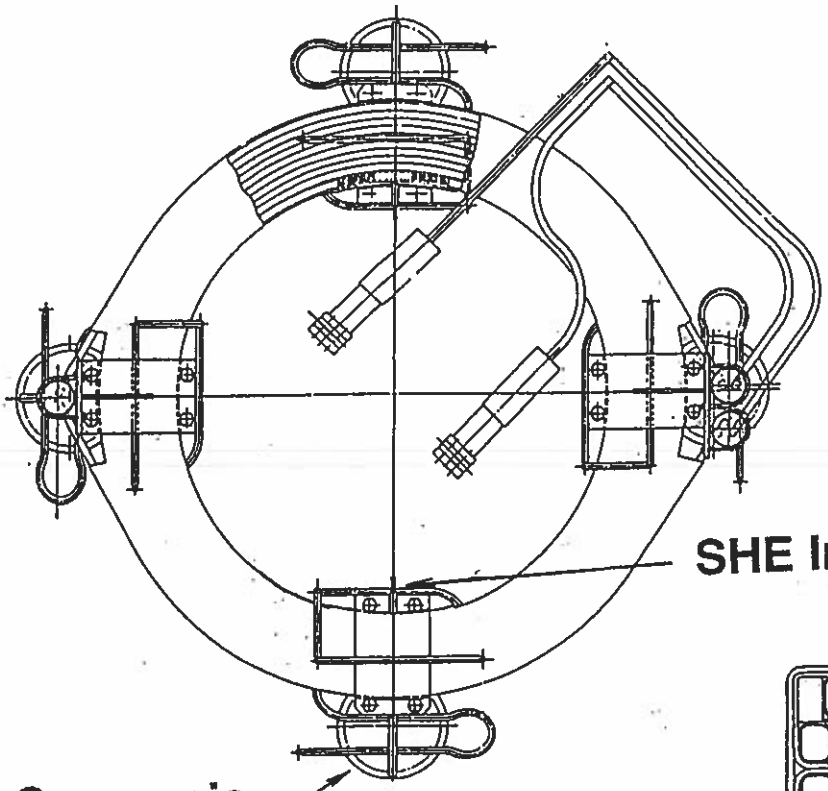

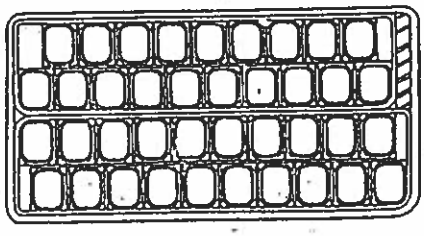

Cross Section
of Winding

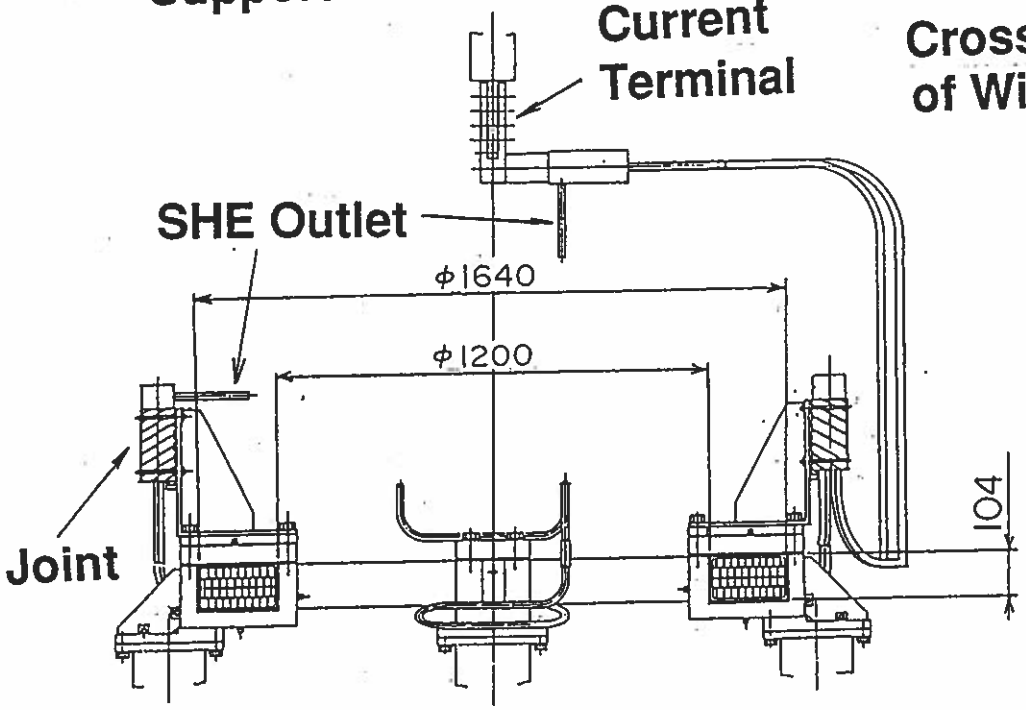

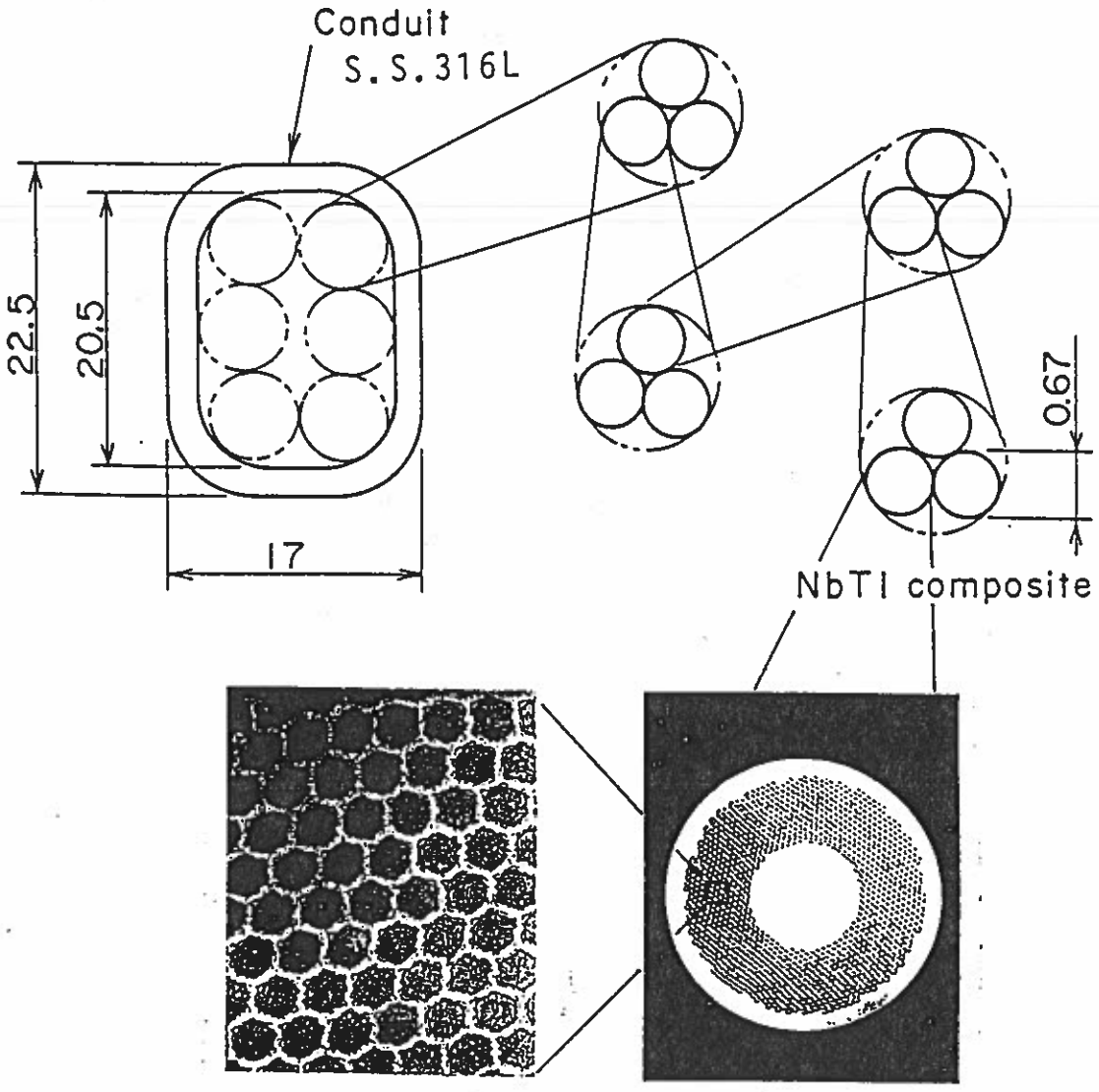
Conduit
S.S.316L
22.5
20.5
17
0.67
NbTI composite
NbTi/Cu/CuNi
1/1.65/0.4
Formvar insulation
0.01mm in thickness

TOKI—PF

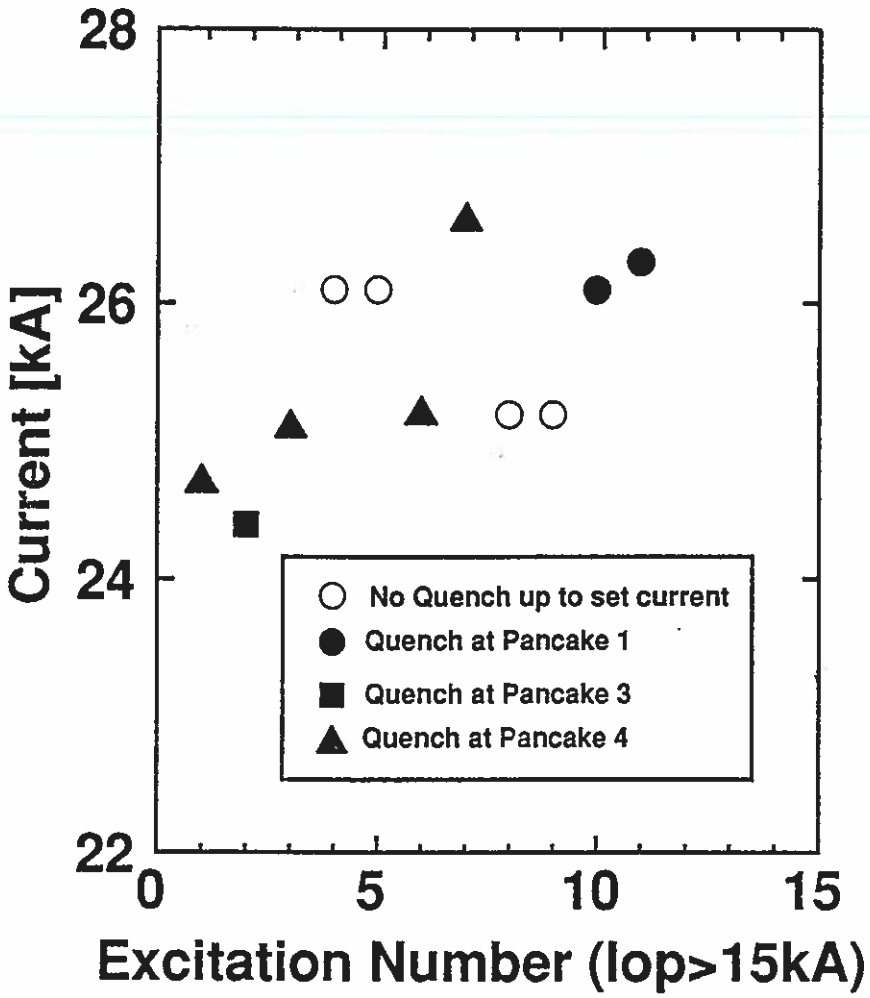
28
26
24
22
Current [kA]
0
5
10
15
Excitation Number (Iop>15kA)
No Quench up to set current
Quench at Pancake 1
Quench at Pancake 3
Quench at Pancake 4

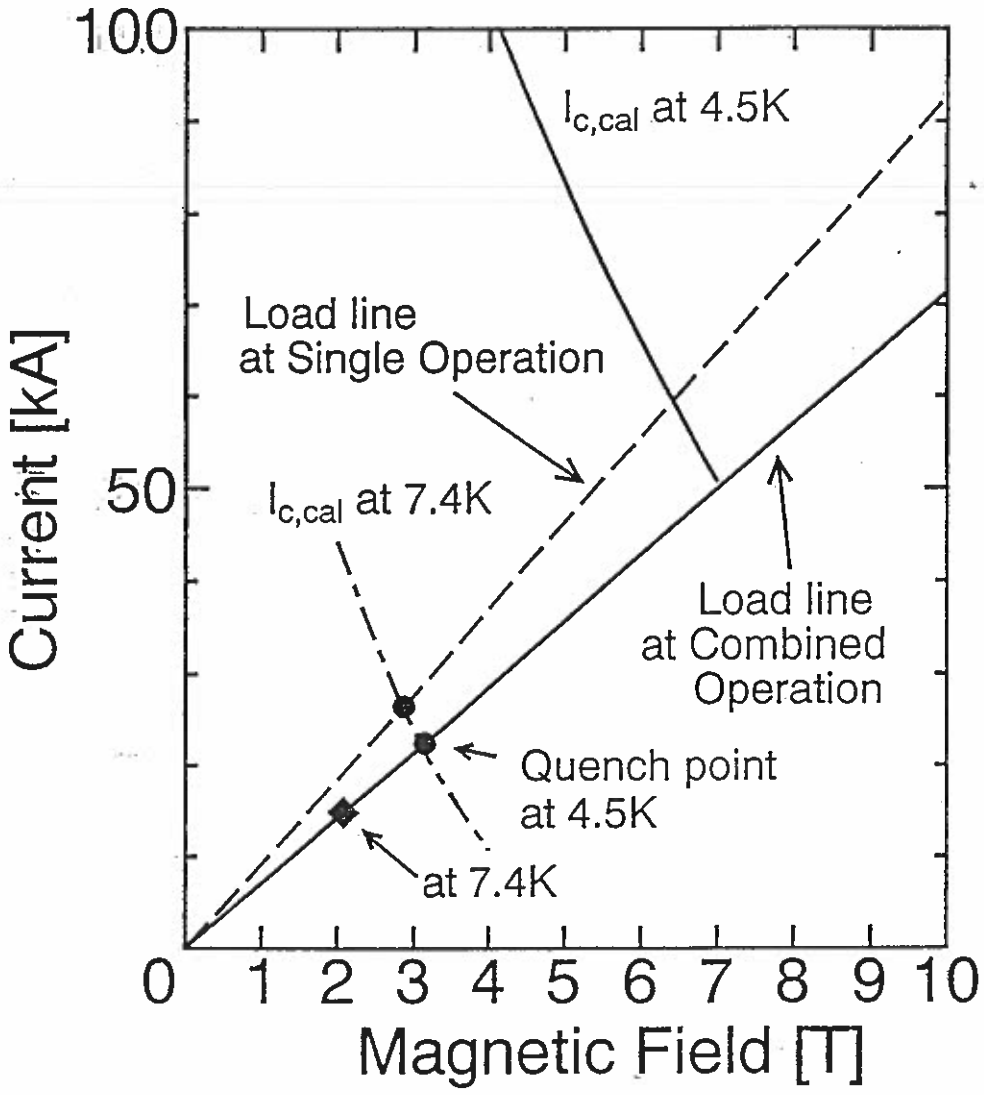

Quench currents of the TOKI–PF coil on the load line

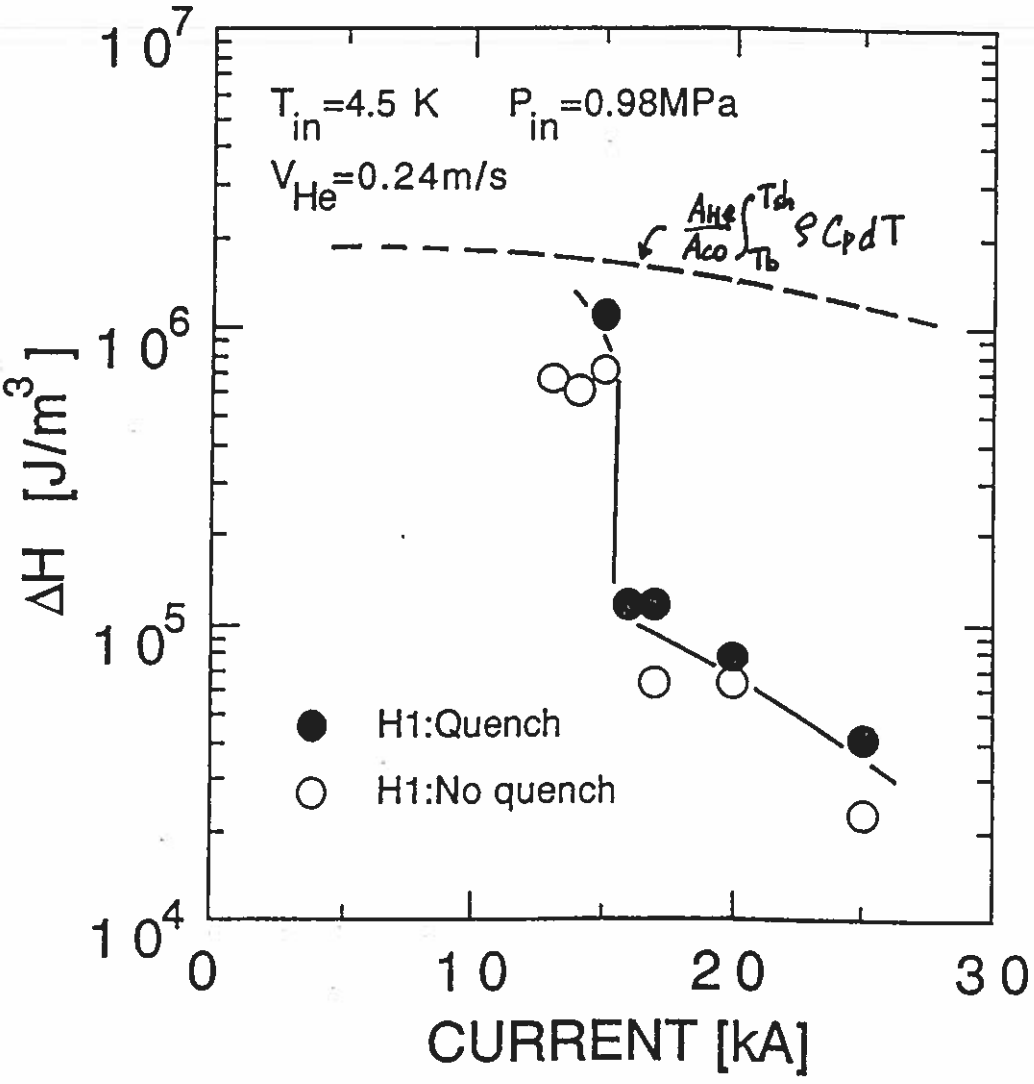
10^7
10^6
10^5
10^4
T_{in}=4.5 K
P_{in}=0.98MPa
V_{He}=0.24m/s
$\frac{A_{He}}{A_{Co}}\int_{Tb}^{Td}\rho C_p dT$
ΔH [J/m^3]
H1:Quench
H1:No quench
0
10
20
30
CURRENT [kA]

Table II
Comparison of the TOKI-PF and IV-S conductors

Conductor	TOKI-PF	IV-S
Type	Cable-in-conduit	Cable-in-conduit
Superconducting material	Nb-Ti	Nb-Ti
Conduit dimension	17.0x22.5 mm^2	17.0x22.5 mm^2
thickness	1.0 mm	1.0 mm
Void fraction	0.40	0.345
Strand diameter	0.673 mm	0.707 mm
Number of strands	486	486
Nb-Ti:Cu:Cu-Ni	1:1.65:0.4	1:2.54:0
Strand surface	Formvar coating(11μm)	Bare

Table III
Principal specifications of the TOKI-PF and IV-S coils

Coil	TOKI-PF	IV-S
Configuration	Two double pancakes	One double pancake
Inner radius	0.6 m	0.6 m
Outer radius	0.82 m	0.76 m
Height	0.11 m	0.052 m
Number of turns	40	16
Cooling method	Forced flow	Forced flow
Operating temperature	>4.5 K	>4.5 K
pressure	<1 MPa	<1 MPa
Number of cooling paths	4 paths	2 paths
Design mass flow rate	16 g/s (total)	10 g/s (total)
Cooling path length	45 mx4	34.5 mx2

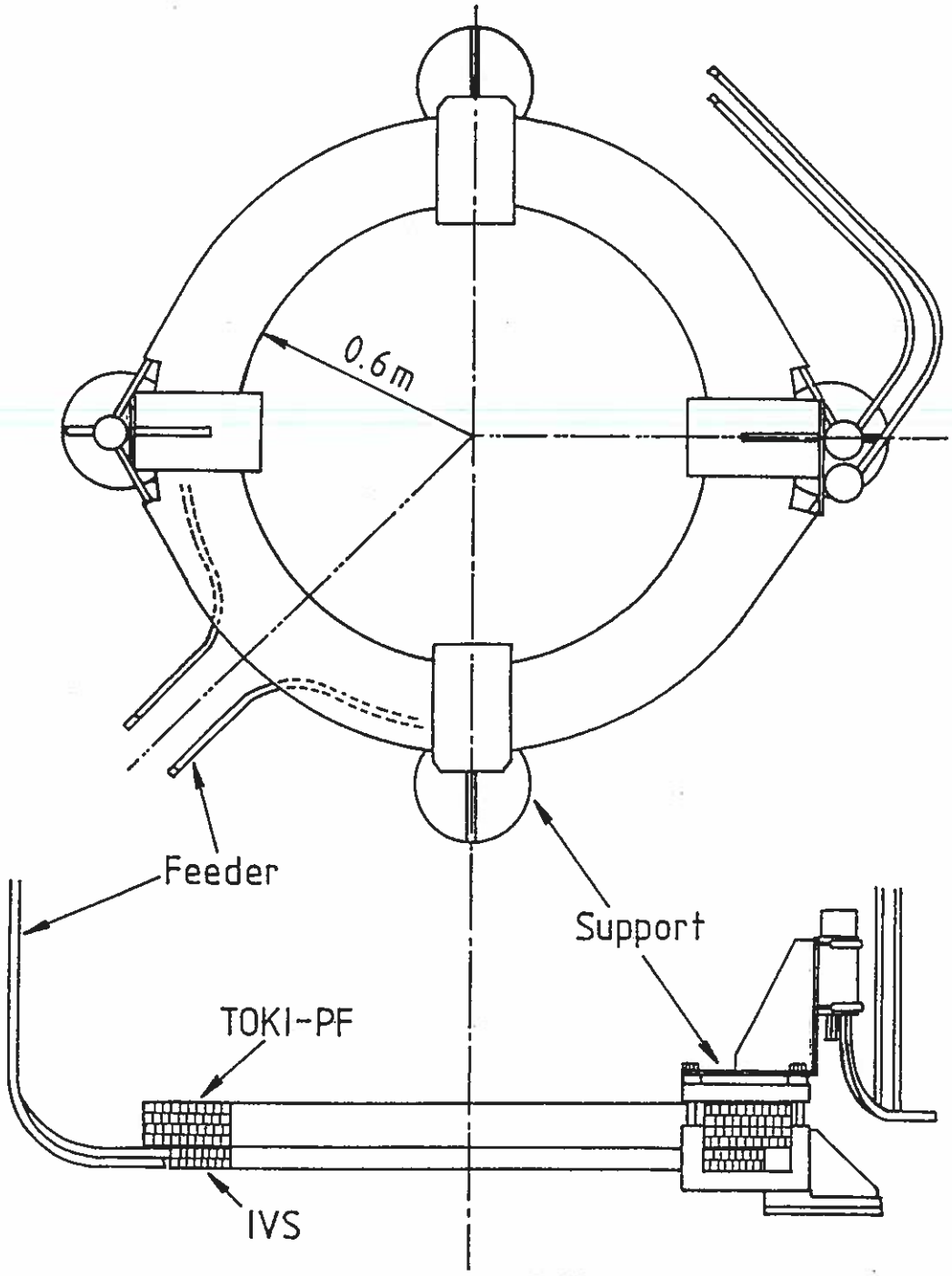

Coil arrangement

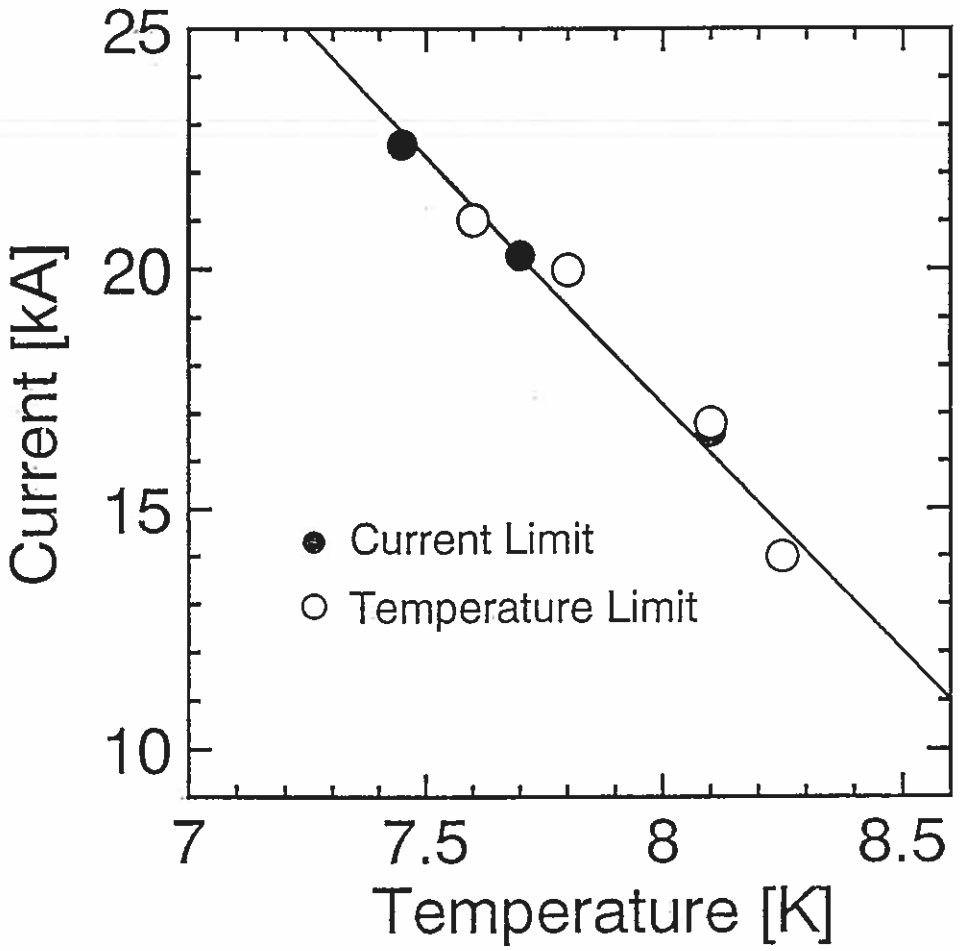

Comparison between the current and temperature limits

$$\Delta H = (1\text{-}f)/f \int_{T_b}^{T_{sh}} \rho_{He} C_p \, dT$$

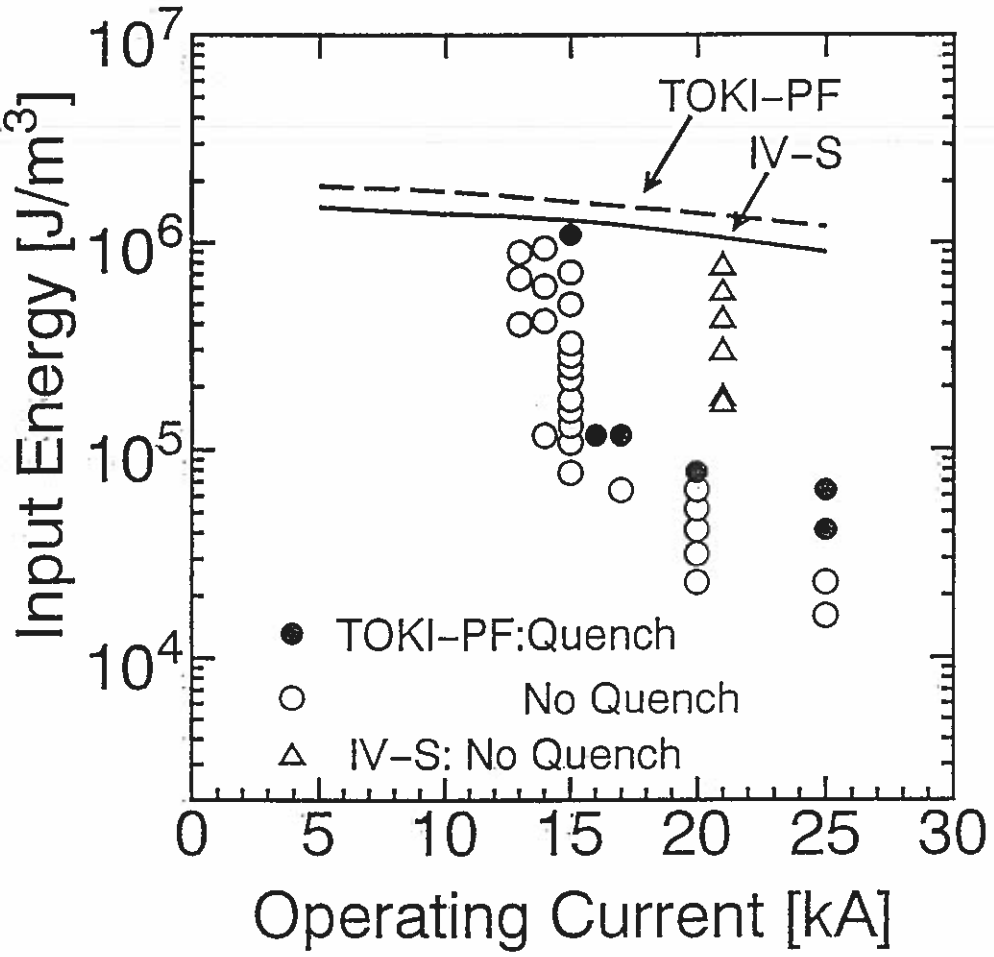

Results of the stability margin measurements at 4.5 K

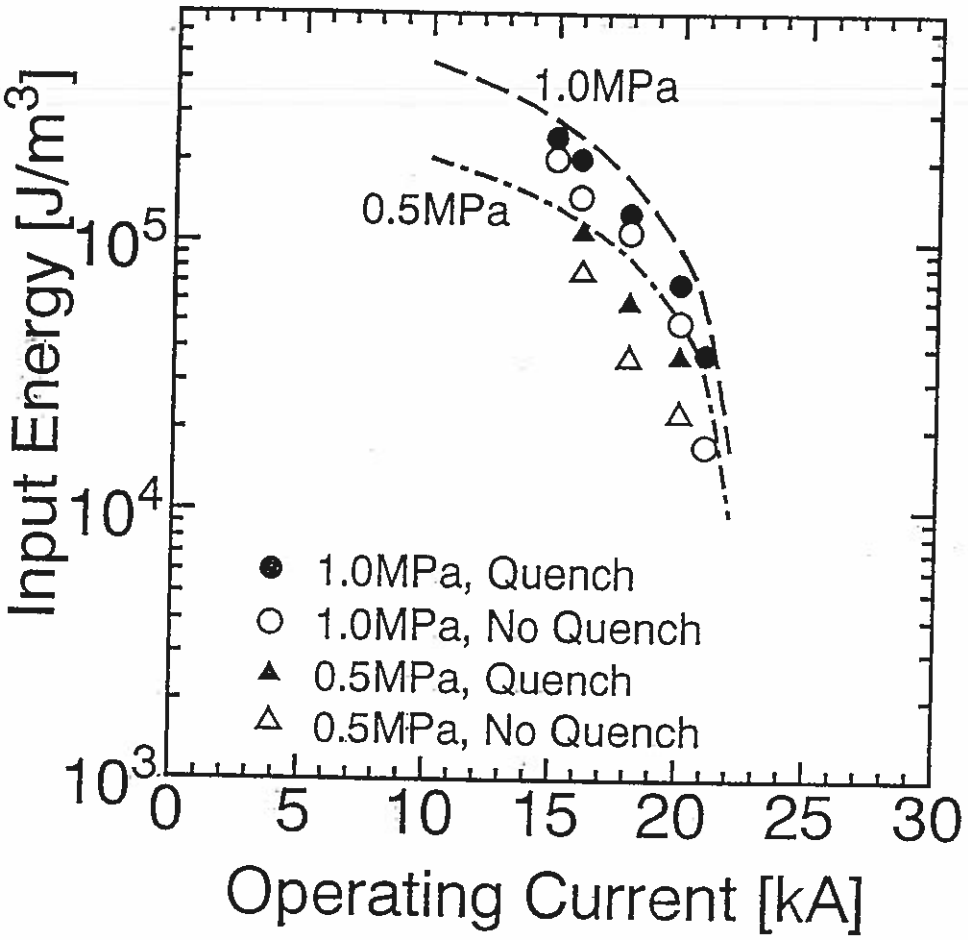

Results of the stability margin measurements at 7.5 K on the IV–S coil.

Table 1. Parameters of conductor for IV-coil.
All dimensions are measured values.

Conduit Dimension	22.9 mm×27.7 mm
Thickness	2.9 mm
Material	SUS316L
Void fraction	38 %
Strand Diameter	0.767 mm
Configuration	$3^4 \times 6$
Cabling pitch: 1st	60 mm
2nd	95 mm
3rd	145 mm
4th	225 mm
5th	408 mm
Strand Composition	1:2.66 (NbTi:Cu)
Resistivity of Copper	4×10^{-10} Ωm at 6.5 T
Filament Diameter	15 μm

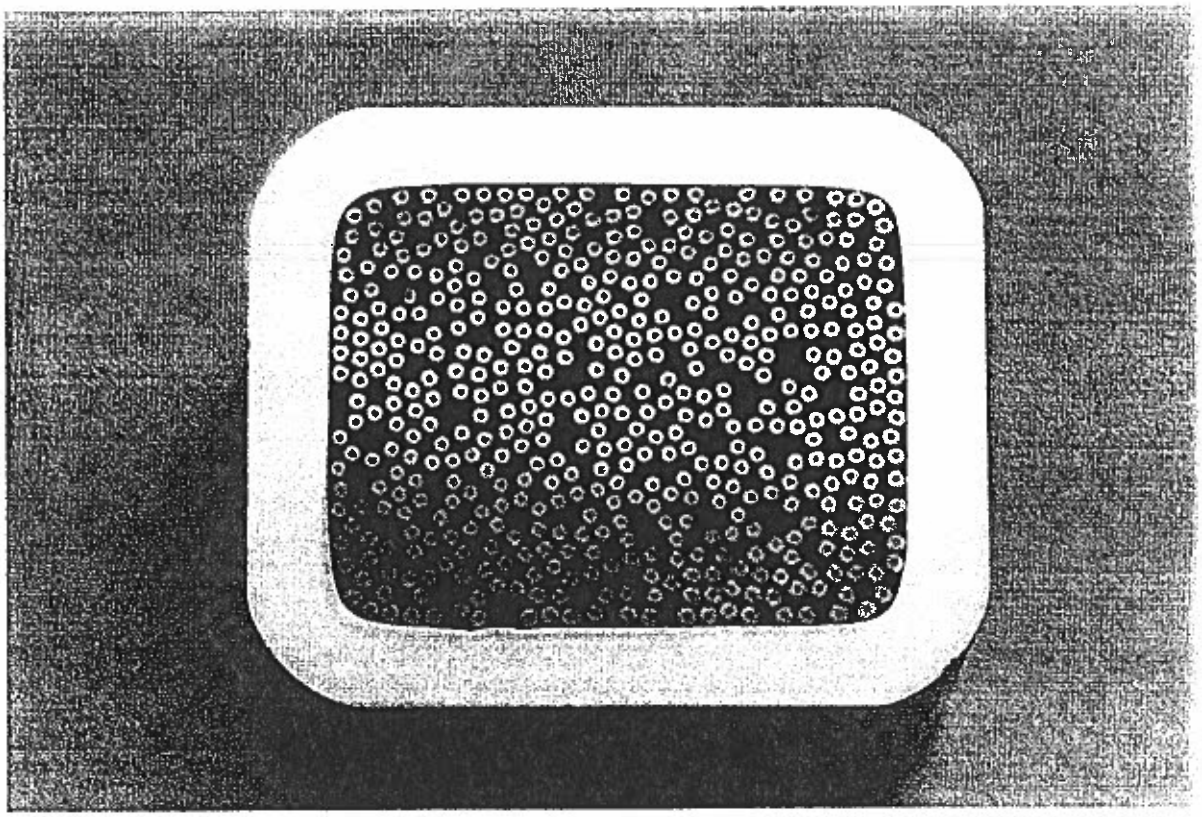

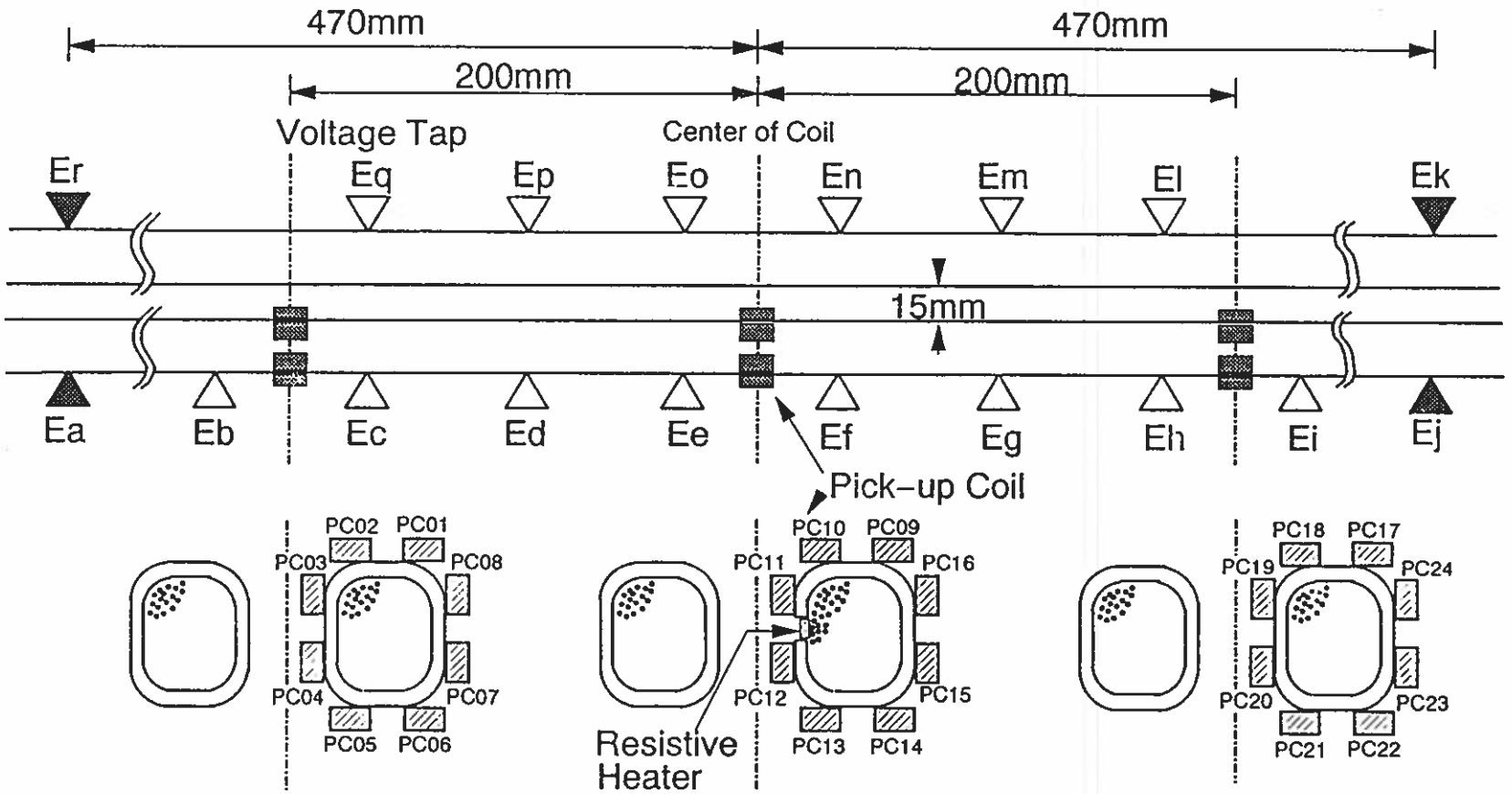
470mm
470mm
200mm
200mm
Voltage Tap
Center of Coil
Er
Eq
Ep
Eo
En
Em
El
Ek
15mm
Ea
Eb
Ec
Ed
Ee
Ef
Eg
Eh
Ei
Ej
Pick-up Coil
PC02
PC01
PC03
PC08
PC04
PC07
PC05
PC06
PC10
PC09
PC11
PC16
PC12
PC15
PC13
PC14
Resistive
Heater
PC18
PC17
PC19
PC24
PC20
PC23
PC21
PC22

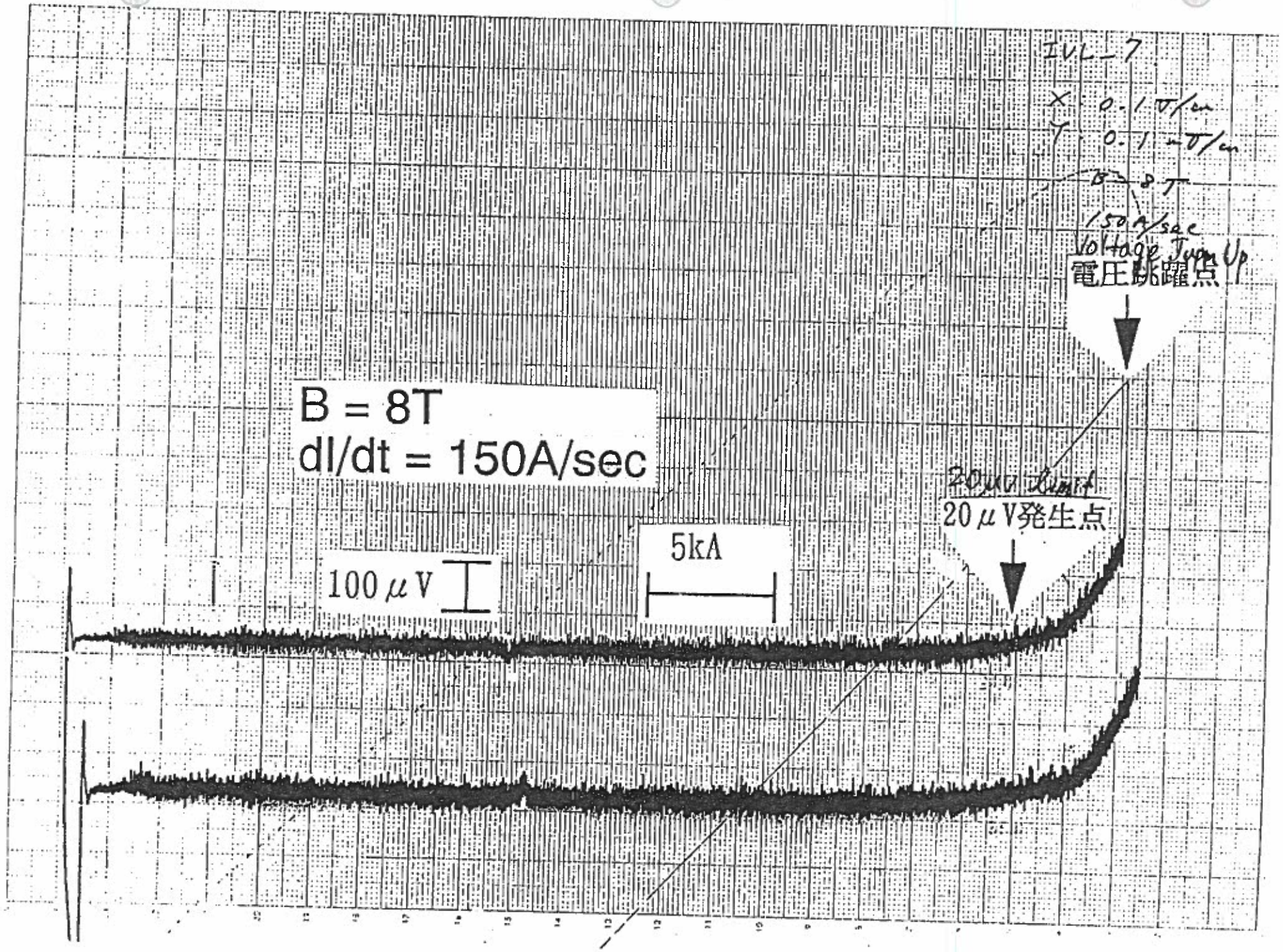
B = 8T
dI/dt = 150A/sec
100 μV
5kA
20μV Limit
20 μV発生点
Voltage Turn Up
電圧跳躍点

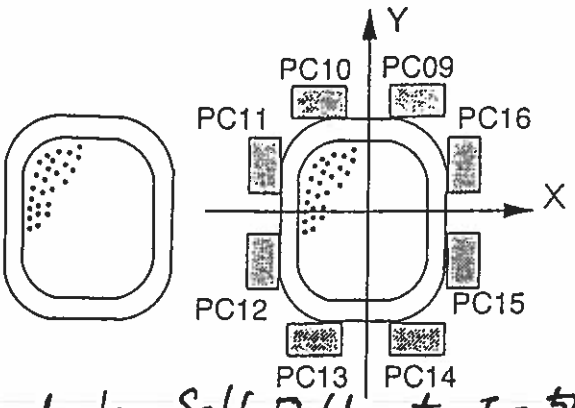

Conductor Self-Field at I = 50kA

50kA通電時の自己磁場

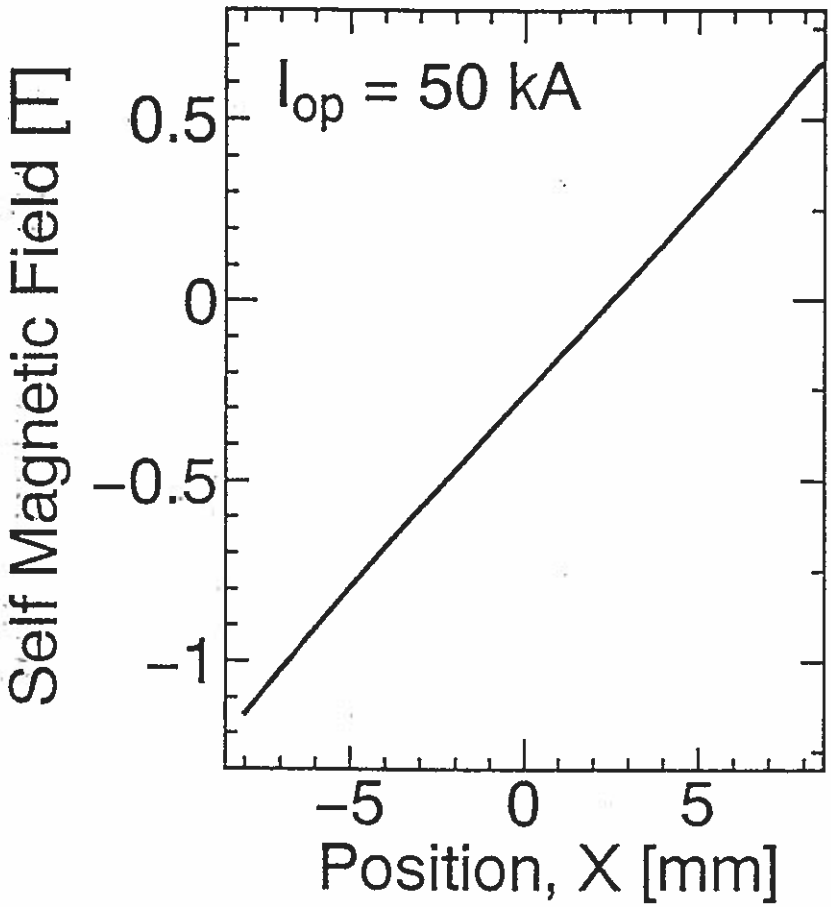

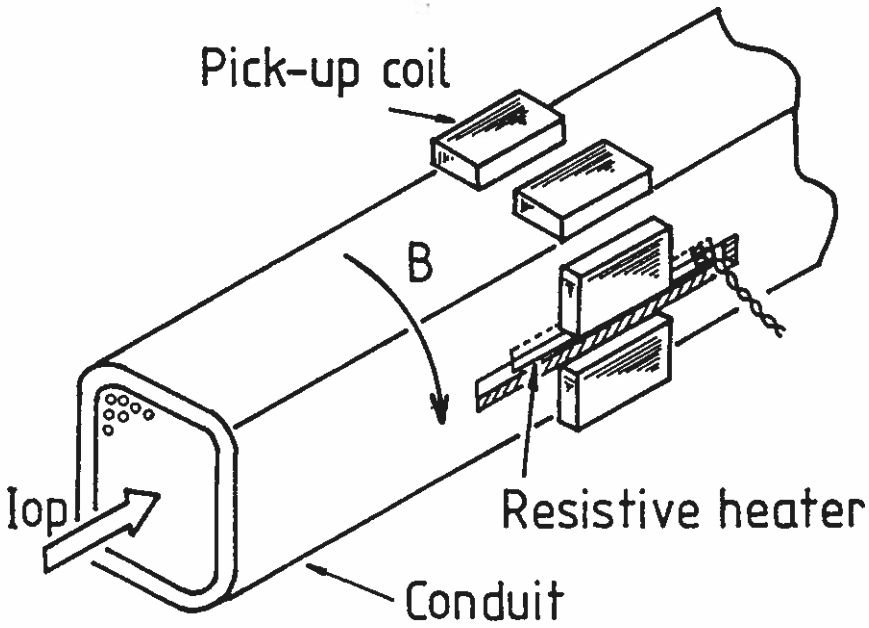
Pick-up coil
B
Iop
Resistive heater
Conduit

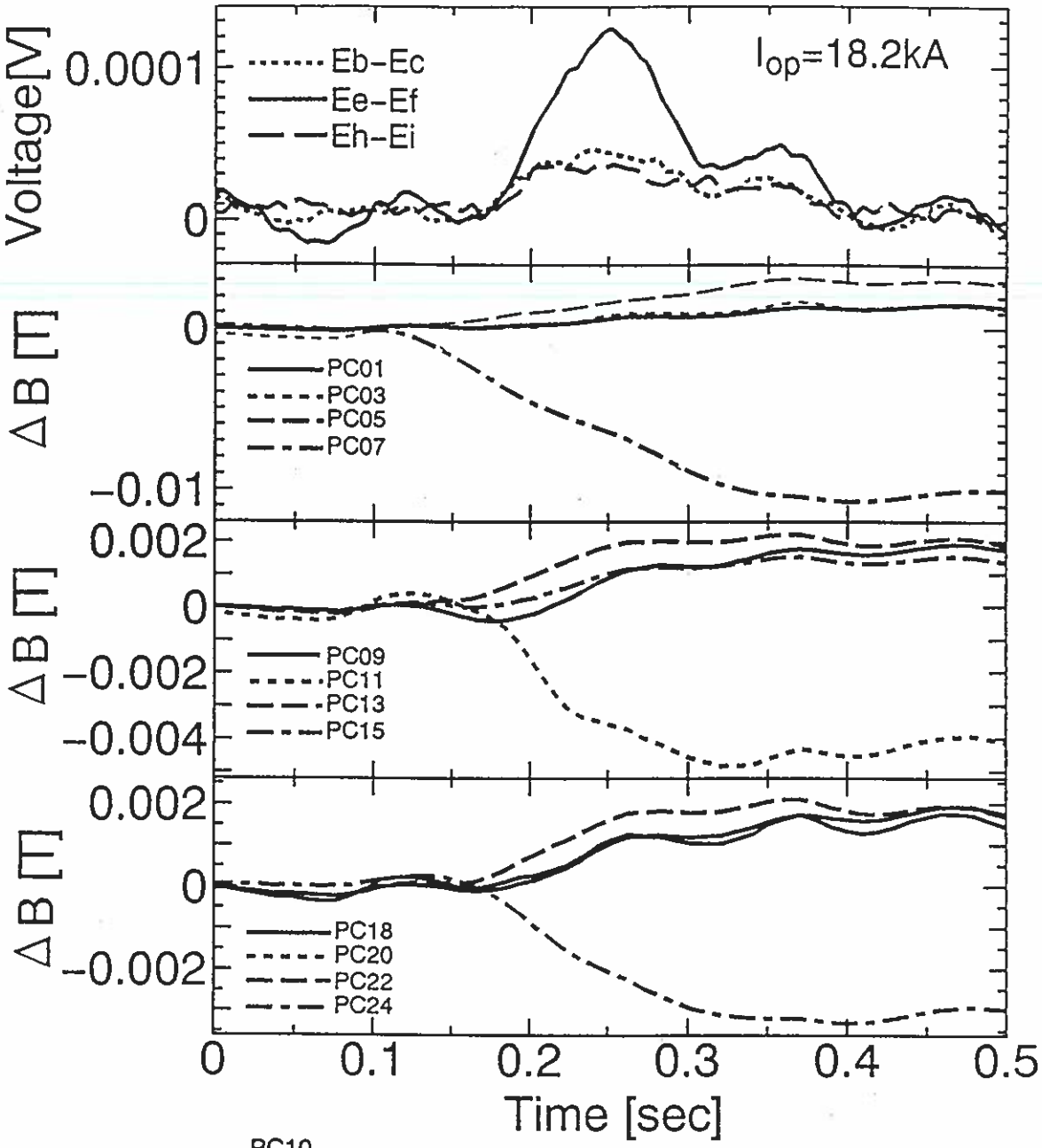
Voltage[V]
0.0001
0
Eb-Ec
Ee-Ef
Eh-Ei
I_{op}=18.2kA
ΔB [T]
0
-0.01
PC01
PC03
PC05
PC07
0.002
0
-0.002
-0.004
PC09
PC11
PC13
PC15
0.002
0
-0.002
PC18
PC20
PC22
PC24
0
0.1
0.2
0.3
0.4
0.5
Time [sec]

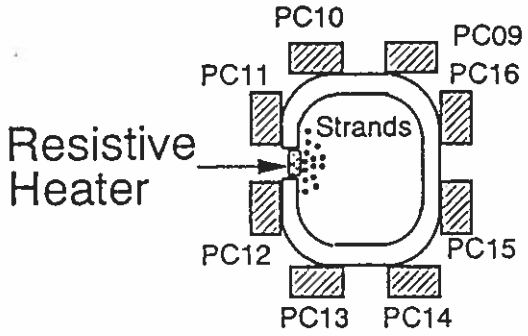
PC10
PC09
PC11
PC16
Strands
Resistive
Heater
PC12
PC15
PC13
PC14

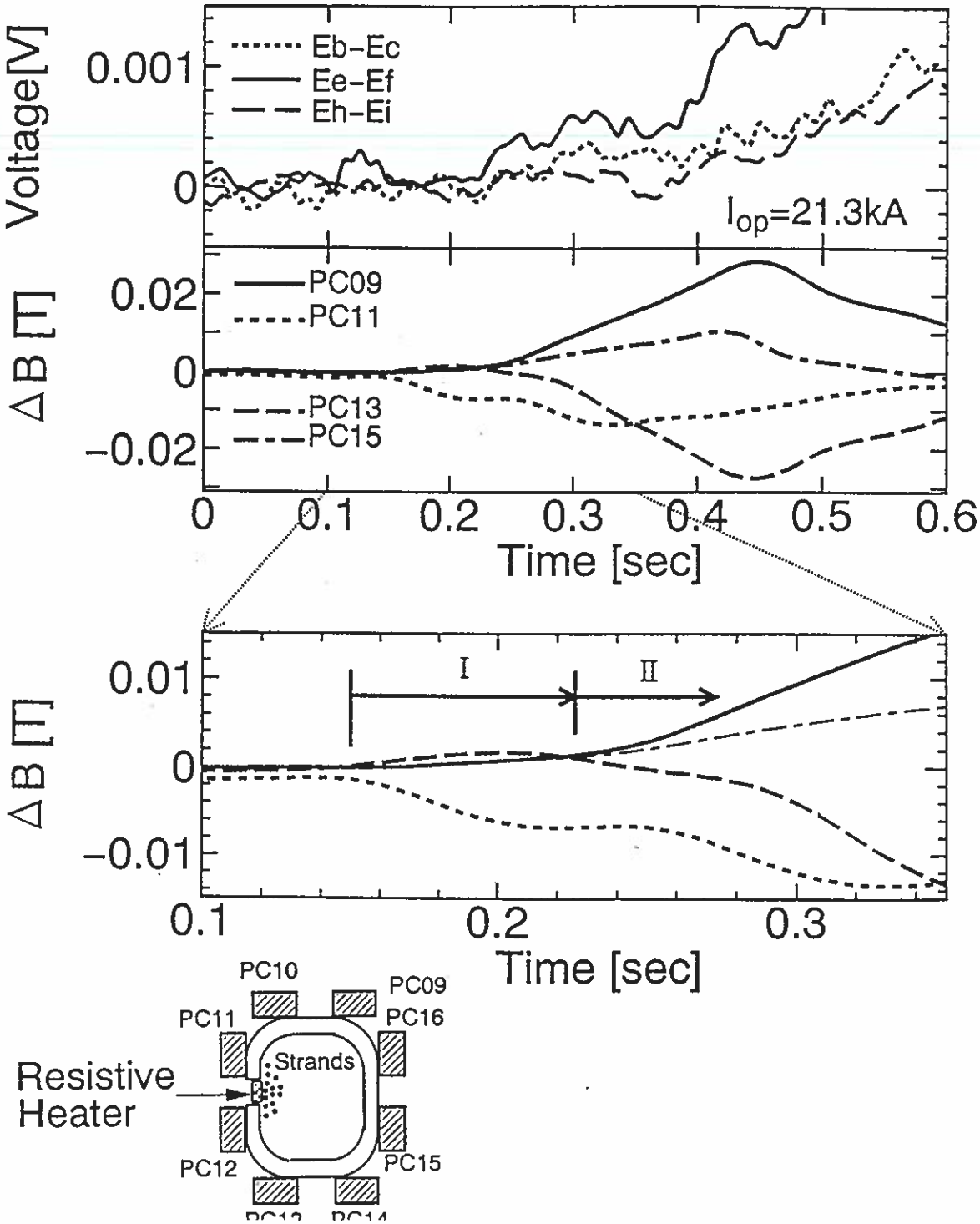
Voltage[V]
0.001
0
Eb-Ec
Ee-Ef
Eh-Ei
I_{op}=21.3kA
ΔB [T]
0.02
0
-0.02
PC09
PC11
PC13
PC15
0
0.1
0.2
0.3
0.4
0.5
0.6
Time [sec]
ΔB [T]
0.01
0
-0.01
I
II
0.1
0.2
0.3
Time [sec]
PC10
PC09
PC11
PC16
Strands
Resistive
Heater
PC12
PC15

Loss Measurement System

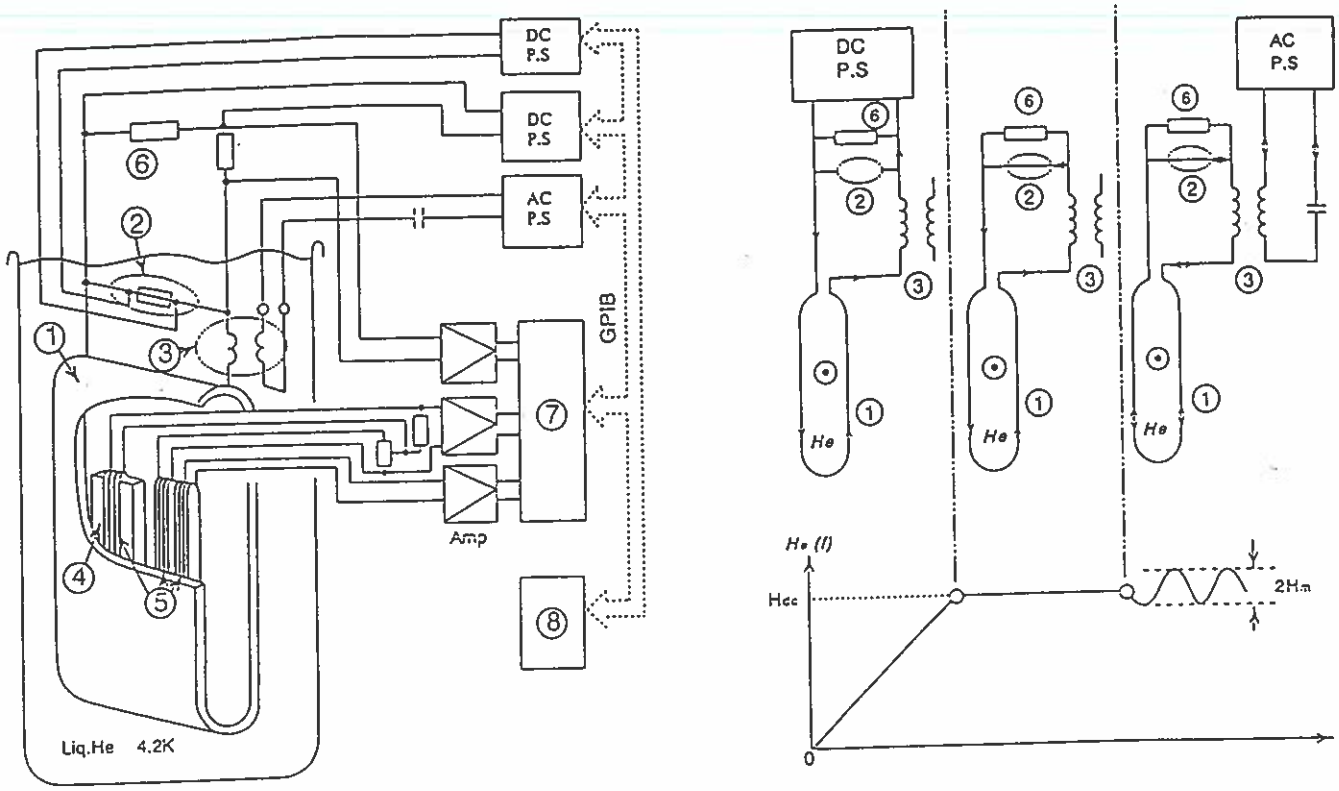

1, A super conducting split magnet; 2, a heat switch; 3a superconducting transformer; 3, a superconducting transformer; 4, a sample conductor; 5, pick-up coils; 6, a dump resistor; 7, A/D converters; 8, a computer. (a) Schematics of the measuring system; (b) sequence of a generation of the small ac magnetic field superposed on the dc field.

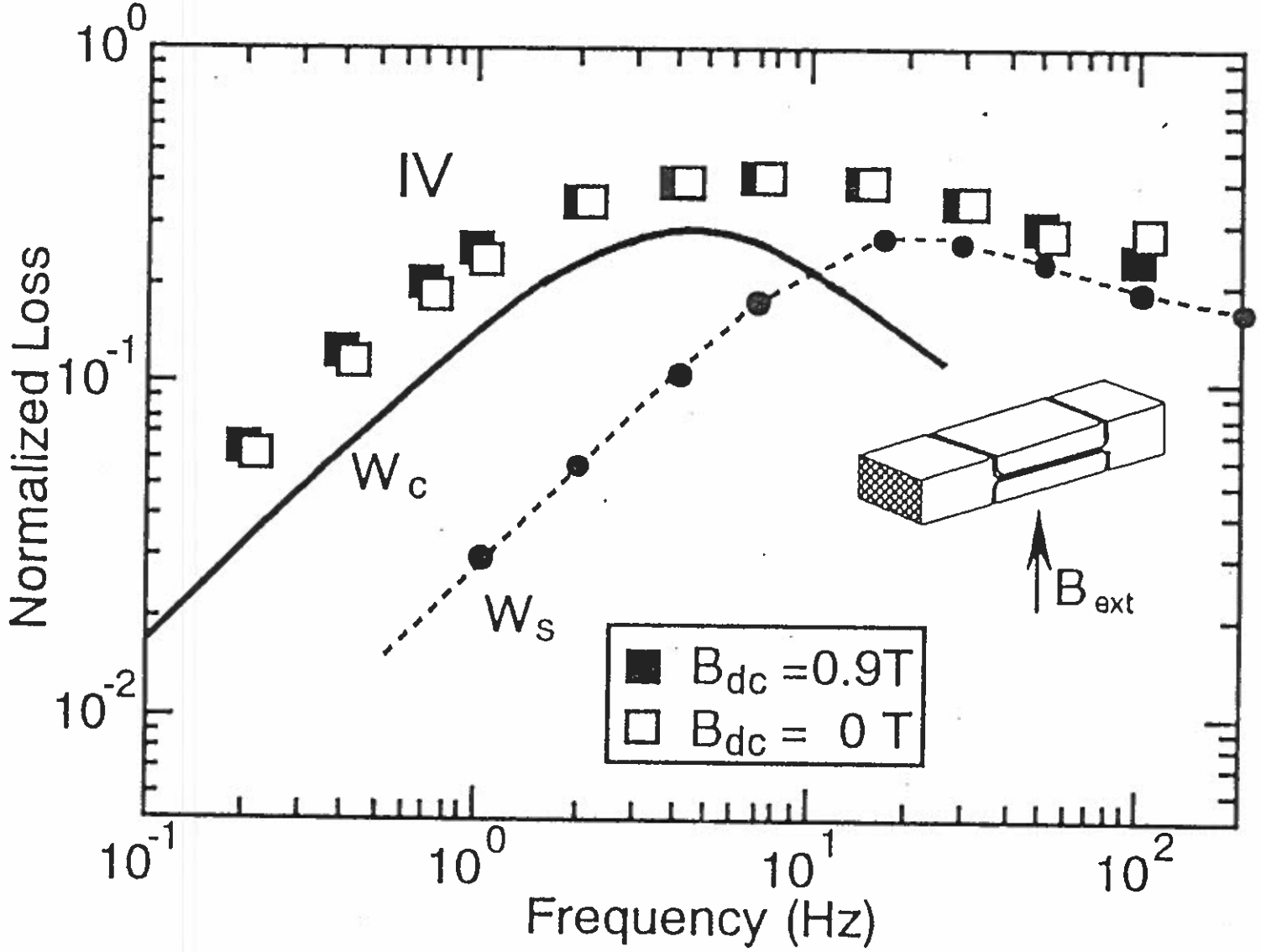
Normalized Loss
Frequency (Hz)
IV
W_c
W_s
B_{ext}
B_{dc} =0.9T
B_{dc} = 0 T
10^0
10^{-1}
10^{-2}
10^{-1}
10^0
10^1
10^2

3. Future R&D Plan

Further researches of the relation between current distribution and stability are necessary.

1. Measurements of the current distribution and stability for short samples of various type cables and conductors.
   - 2 or 3 strands cable -- for basic study
   - Compacted strand cable -- changing surface treatments
     (collaboration with KEK)
   - CICC including Nb_3Sn conductors

2. Measurement of AC loss under the coil condition
   - AC loss measurement of the IV coil
   - AC loss measurement of short sample conductors carrying DC transport current
     (collaboration with Kagoshima University)

4. Summary

1. Development of forced-flow cooled superconducting poloidal coils for LHD has been successfully done making importance on stability.

2. The stability of an R&D coils and conductors were improved by removing the insulation of strand and increasing stability of a strand.

3. The current re-distributions, when a part of strands became normal, were observed in short sample tests of IV conductor using pick-up coils.

4. High stability of a NbTi CICC with bare strands is caused by its smooth current re-distribution characteristics

5. The inter-strand coupling loss of bare strands CICC was about 10 times larger than a single strand loss.

6. The optimization of Stability and AC loss is next item to be studied.

ion Engineering and Design 20 (1993) 161–166
rth-Holland

Experimental results of the R&D forced-flow poloidal coil (TOKI-PF)

K. Takahata[a], T. Mito[a], N. Yanagi[a], M. Sakamoto[a], A. Nishimura[a], S. Yamada[a], J. Yamamoto[a], S. Mizumaki[b], K. Nakamoto[b], K. Yamamoto[b], T. Yoshida[b], H. Itoh[b], M. Shimada[b], Y. Wachi[b] and H. Shinohara[b]

[a]*National Institute for Fusion Science, Nagoya 464-01, Japan*
[b]*Toshiba Corporation, Chiyoda-ku, Tokyo 100, Japan*

As research and development (R&D) of poloidal-field coils for the Large Helical Device (LHD), a forced-flow cooled cable-in-conduit-type NbTi superconducting coil (TOKI-PF) has been tested. The success of excitations assured us that the NbTi cable-in-conduit conductor can be adopted for the LHD poloidal coils. During cool-down, mainly the hydraulic characteristics were measured. The friction factor could be expressed by using an empirical formula. In the DC operations, training behavior was observed, like in a pool-cooled coil. The friction factor was also affected by the number of excitations, which may be related to strand movement. The stability margin and propagation velocity were also measured using an inductive heater. It became evident that the stability margin had a lower value when the operation current was higher than 15 kA. This current seems to correspond to the limiting current.

1. Introduction

The Large Helical Device (LHD) is a heliotron/torsatron-type experimental fusion device and the seven-year project for construction started in 1990 [1]. Before starting the machine construction, various R&D programs have been carried out since 1988. The TOKI-PF coil was fabricated as one of the R&D coils in order to confirm the reliability of a forced-flow cooled NbTi coil and to obtain the fundamental data for design of the LHD, such as a friction factor, stability margin, normal zone propagation velocity [2]. In the current design of the LHD, forced-flow cooling has been adopted as the cooling method for the poloidal coils. To simulate the poloidal coils, a cable-in-conduit-type conductor with a nominal current of 25.6 kA at 7 T was used as conductor of the TOKI-PF coil. One of the LHD poloidal coils (IV coil) is charged up to 20.8 kA in half an hour, producing a maximum field of 6.5 T. A NbTi cable-in-conduit-type conductor is planned to be used for the IV coil. The other poloidal coils are now under design. The results of R&D affect the possibility of adoption of a cable-in-conduit conductor.

In August 1991, the first step of the excitation tests was completed. The coil was cooled down and warmed up three times, and the hydraulic characteristics were examined. In the excitation tests, DC operations and stability margin measurements were performed. In this paper, an outline of the results will be described and the design criterion of the LHD poloidal coil is shown.

2. *Experimental arrangement*

The TOKI-PF coil consists of two double pancakes. The principal specifications of the coil and the conductor are listed in table 1. Supercritical helium was shared between four parallel cooling paths as shown in fig. 1. The rated mass-flow rate was 4 g/s per path with a pressure of 0.98 MPa. Thermometers, flow meters and pressure taps were attached to the inlet and outlet paths in order to measure the hydraulic characteristics. The locations of the sensors are also presented in fig. 1. A resistive heater attached to the inlet of the first pancake was used to raise the temperature of the helium in stability tests. The output signals of the sensors were fed to a computer, Hewlett-Packard

Correspondence to: Dr. K. Takahata, National Institute for Fusion Science, Nagoya 464-01, Japan.

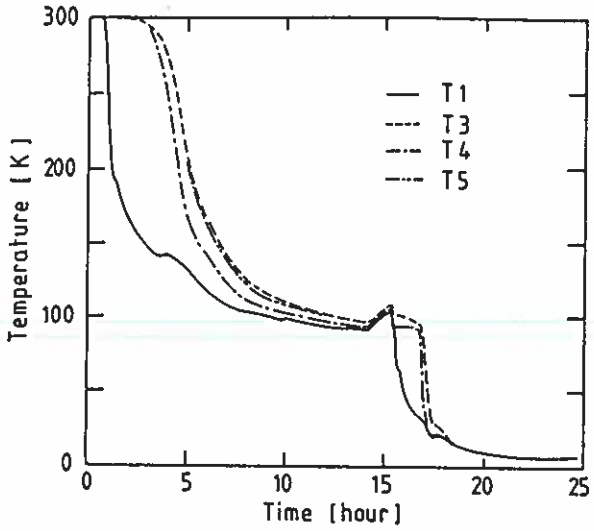

Fig. 3. Cool-down curves showing the inlet (T1) and outlet (T3–5) temperatures of helium.

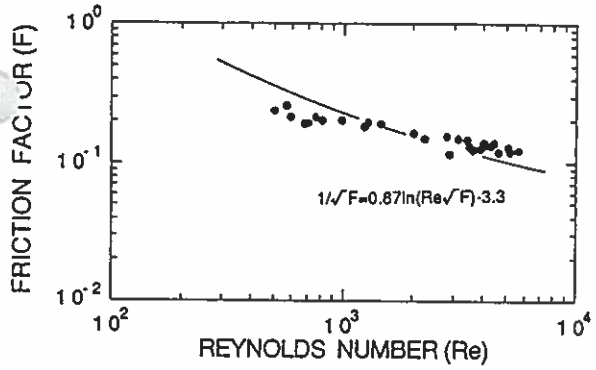

Fig. 4. Friction factor of the TOKI-PF versus Reynolds number. The solid line is a fitted curve using an empirical formula.

where ρ, u, L and D_h are the density, velocity of the fluid, length of the path, and hydraulic diameter, respectively. The hydraulic diameter of this conductor was calculated to be 0.5 mm. The solid line is a fitted curve using the empirical formula [4,5]:

$$1/\sqrt{F} = 0.87 \ln(\mathrm{Re}\sqrt{F}) - A\,, \qquad (2)$$

where A is a coefficient depending on the wall roughness. This formula can be applied to the conductor design for the LHD poloidal coils.

3.2. DC excitation tests

As the first step of the excitation tests, DC operations were performed with a rated mass-flow rate of 4 g/s/path. The current sweep rate was set to be from 8 to 200 A/s. The coil achieved the nominal current of 25.6 kA after experience with three premature quenches. Figure 5 displays the quench behavior. The horizontal axis shows the number of excitations over 15 kA (N_{ex}). The quench locations are also shown in the figure. It was found that the quench currents had a tendency to increase with increasing the number of excitations, and the quench locations were not limited. Although some reasons can be considered for the quench, this training behavior indicates the possibility of mechanical disturbances, e.g. strand movements in the conduit [6].

The effect of strand movements appeared in the hydraulic characteristics. Figure 6 shows the variation of the friction factor with the current in the coil. N_{ex} in

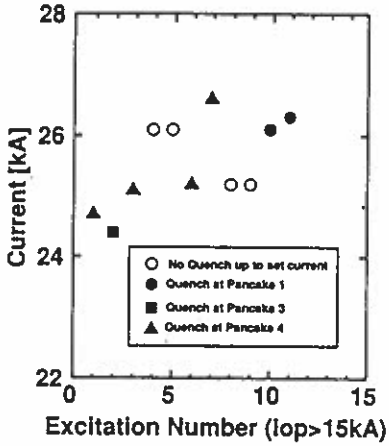

Fig. 5. Quench behavior in DC excitation tests. The open circles are set currents when the excitation had succeeded without quench. The closed symbols are quench currents.

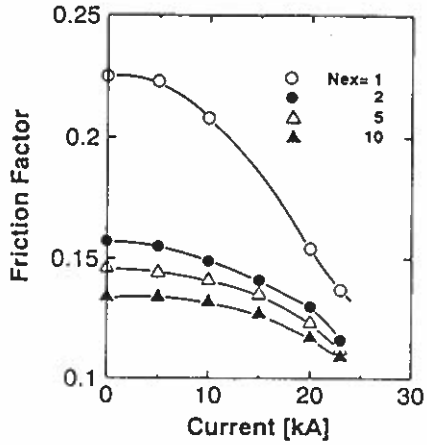

Fig. 6. Variations of the friction factor with current during excitation. N_{ex} indicates the number of the experiment.

Table 1
Principal specifications of the TOKI-PF coil

Conductor		Coil	
Type	Cable-in-conduit	Configuration	Two double pancakes
Superconducting material	NbTi	Inner radius	0.6 m
Critical current	50 kA at 7 T	Outer radius	0.82 m
Conduit dimension	17.0 × 22.5 mm	Height	0.11 m
Void fraction	0.4	Operating current	25.6 kA at 2.76 T
Strand diameter	0.67 mm with formvar (10 μm)	Number of turns	40
Number of strands	486	Inductance	3.18 mH
NbTi:Cu:CuNi	1.0:1.6:0.5	Stored energy	1.04 MJ

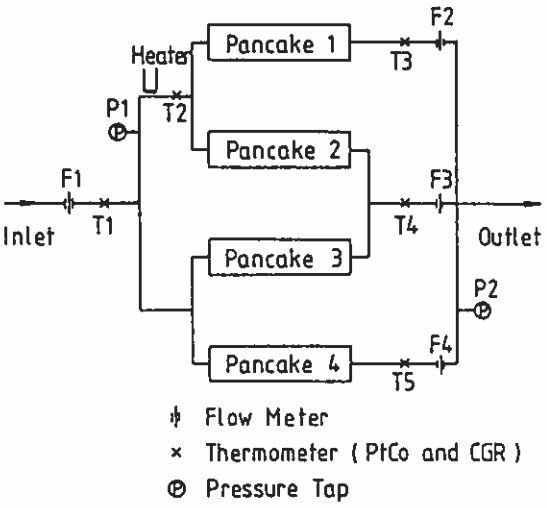

Fig. 1. Schematic flow diagram and sensor location for measuring the hydraulic characteristics.

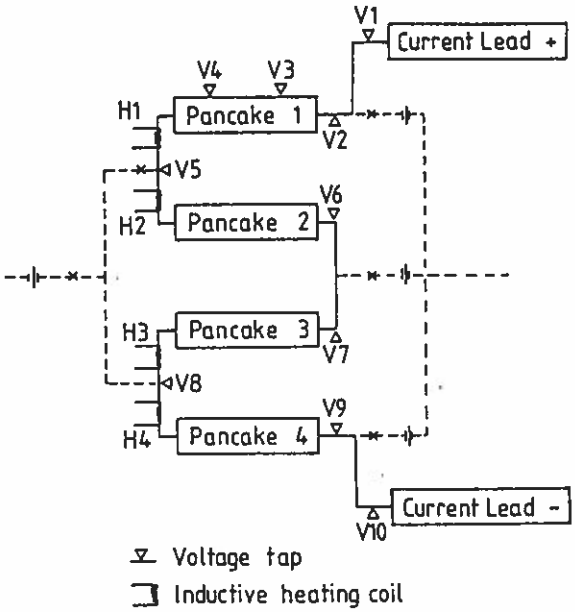

Fig. 2. Schematic current path and locations of the voltage taps and inductive heaters.

(HP) 360 with HP3852 data acquisition units, and the state of the helium was calculated automatically using the program package for the thermophysical properties "PROPATH version 7.1" [3]. We could get analog inputs with 48 channels, and a maximum sampling rate of 100000 ch/s using 13-bit analog/digital converters. The data acquisition system could check important information immediately during operation. Figure 2 shows the current path and the locations of the voltage taps. Inductive heaters with a length of 0.1 m with 200 turns were attached to each pancake in order to apply a thermal disturbance. The power supply for the inductive heater consists of silicon controlled rectifiers, a capacitor bank of 0.4 mF, and a 1 kV–80 mA charging supply. In actual tests, current discharges were obtained with an oscillation frequency of 500 Hz and a decay time constant of 5 ms, and they put an energy into the conductor of up to 1 MJ/m^3.

3. Results and discussion

3.1. Cool down

The coil was cooled down and warmed up three times. The total cooling weight is about 1300 kg. Figure 3 shows the second cool-down curves. Helium gas of 90 K was supplied to the coil during the first 15 h. The coil was then cooled down to 4.5 K by helium gas of 1 MPa, 40 g/s within 10 h.

The pressure drop (Δp) is shown in fig. 4. as the friction factor (F) versus the Reynolds number (Re). The friction factor is defined by Darcy's equation [4]:

$$\Delta p = F(\rho u^2/2)(L/D_h)\,, \qquad (1)$$

the figure indicates the number of excitations. The friction factor decreased with increasing operating current. This may be the reason that the strands were shifted outward in the coil due to the electromagnetic force. In the conduit, narrow gaps seemed to be formed due to the eccentricity of the strand bundle. The creation of narrow gaps causes an increase of the hydraulic diameter and a decrease of the friction factor. Figure 6 indicates that the friction factor also depends on the number of excitations. The friction factor was replotted as a function of the number of excitations, as shown in fig. 7. The friction factor showed a decreasing tendency with the number of excitations. This means that the strands were moved during excitation and partially fixed at stable positions after the discharge. The training behavior described before can be explained qualitatively by these phenomena. Although it may be quite allright to consider that the quenches were due to the strand movements, we could not observe voltage spikes due to the strand movements. The scan frequency of the data acquisition (250 Hz) may be smaller than the voltage oscillation due to the strand movement; about 10 kHz [7].

3.3. Stability tests

If the stability margin of the conductor had exceeded the heat discharge due to the strand movement, the quench might have been avoided. The stability margin was thus examined by using an inductive heater, and the results are shown in fig. 8 as a function of operating current (I_{op}). It was clear that the stability margin has a lower value, 10^5 J/m^3 or less, when the operation current was higher than 15 kA. The dashed curve in the figure is the helium

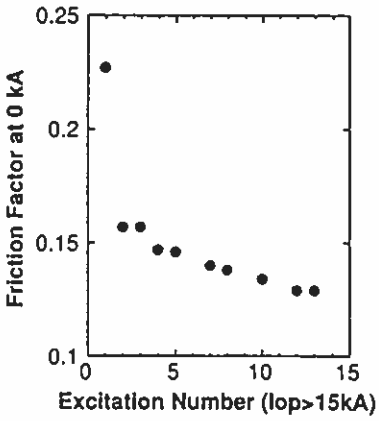

Fig. 7. Dependence of the friction factor on the number of excitations just before excitation.

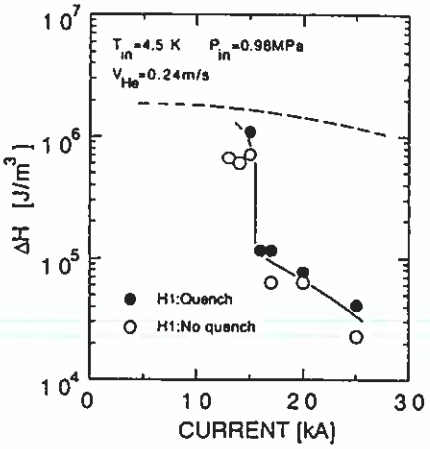

Fig. 8. Variation of the stability margin with current measured by using the H1 heater. The dashed line is the calculated helium enthalpy.

enthalpy, calculated as [8]

$$\Delta H = (1-f)/f \int_{T_b}^{T_{sh}} \rho_{He} C_p \, dT \,, \tag{3}$$

where f is the volume fraction of conductors inside the cable space, T_b and T_{sh} are the bath and current sharing temperature, respectively, ρ_{He} is the helium density, and C_p is the specific heat at constant pressure of helium. The stability margin at $I_{op} < 15$ kA was about 10^6 J/m^3, which was in agreement with the helium enthalpy. On the other hand, the boundary between the upper and lower stability seems to correspond to the limiting current (I_{lim}) which has been observed in previous studies. Lue and Miller [8] empirically evaluated the limiting current. Since their empirical equation is adopted in this work, I_{lim} is expressed by the relationship,

$$I_{lim} = 0.23\, k (T_c - T_b)^{1/2} \rho_{Cu}^{-1/2} \,, \tag{4}$$

where T_c is the critical temperature of the superconductor and ρ_{Cu} is the resistivity of the copper stabilizer. These parameters depend on I_{op} because the magnetic field is proportional to I_{op}. Miller [9] pointed out that the coefficient k depends on the initial pressure of helium and examined the dependency for the range 0.3 to 0.6 MPa. In this work, k is assumed to be 0.8 at 0.98 MPa. In this work, k is assumed to be 0.8 at 0.98 MPa by extrapolation. The calculation shows that the I_{lim} of the coil is 22 kA. The measured value was lower compared to the calculated one. The first reason may be decrease of the heat transfer coefficient

due to the formvar insulation of 0.01 mm in thickness. We consider that the unevenness of the initial current distribution in the conductor is another reason, because the strands were insulated and the current must have transferred at only the ends of the conductor.

3.4. Normal propagation

Figure 9 shows typical pancake voltage profiles at $I_{op} = 15$, 20, and 25 kA in the stability tests. The quench was induced by the inductive heater (H1) and the current was dumped when the normal voltage exceeded 0.1 V for 0.1 s. The normal voltage of 0.1 V corresponded to a normal zone length of 3 m at I_{op} = 20 kA. Note that the voltage increased after a while since the heater was on. In the case of 15 kA, the delay time came up to 1 s. Figure 10 shows the normal-zone length as a function of time, estimated from the voltage profiles in fig. 9. In this calculation, the increase in the resistivity of copper was disregarded as the first assumption. Previous studies [10–12] reported that the length is proportional to a power n the time. The n values are also indicated in fig. 10. Dresner [10] evaluated the n value to be 1.33 in an analysis. Wachi et al. [11] and Ando et al. [12] experimentally obtained an n value of 1.04–1.46 and 1.6, respectively. Our data in the case of a lower current was higher compared with the previous studies; n = 2.35 at 20 kA, 2.65 at 15 kA. The results mean that the quench delayed from the heat discharge but the subsequent normal-zone growth was relatively faster.

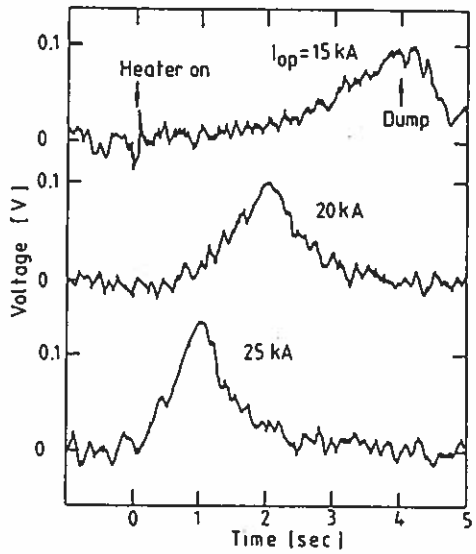

Fig. 9. Typical voltage profiles between the taps V2 and V5 as the coil quenched due to H1 heater.

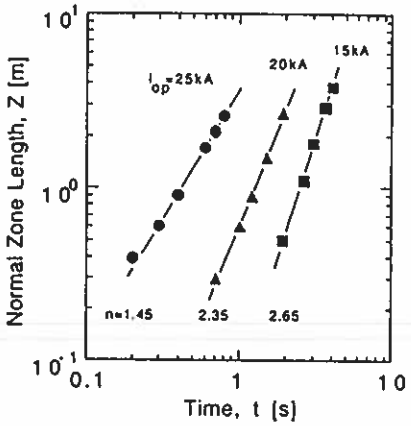

Fig. 10. Normal-zone length as a function of time estimated from the pancake voltage.

The behavior of the quench is now under study by using numerical analyses. However, the non-uniform distribution of the current may be related to the quench behavior; some strands which have higher current density quench at the first stage and whole strands subsequently quench due to the Joule heating of the initially quenching strands

3.5. Design of the conductor for the LHD poloidal coils

The cable-in-conduit conductor will be adopted for the LHD poloidal coils. The experimental results of the TOKI-PF coil contributed to the design of the actual conductor. The major issues revealed were the strand movements and the unevenness of the current distribution. For the actual conductor, the void fraction and cabling pitch will be reduced to as small as possible in order to avoid strand movement. The basic policies for avoiding current unevenness are to remove the resistive layer on the strand surface and to improve the conductor connection using diffused junction between filaments. In order to obtain a higher stability margin, we planned that (1) CuNi is not added to the strand, (2) the copper/NbTi ratio is increased to 2.7, (3) the nominal/critical current ratio is increased to about 3, and (4) the copper resistivity is reduced to as small as possible. The limiting current is expected to be more than 25 kA.

4. Conclusion

A forced-flow cooled NbTi coil (TOKI-PF) was tested and useful data were obtained for the design

and construction of the LHD poloidal coils. A summary of the results is shown below.

(1) The pressure drop was examined as a function of the Reynolds number and expressed using an empirical formula.

(2) In DC operations, training behavior was observed. The origin of quench seems to be strand movement, which was proved from the hydraulic characteristics.

(3) The stability margin shows a rapid decrease at 15 kA. This current seems to correspond to the limiting current which has been observed in previous studies. The value of 15 kA was, however, lower compared to the calculation using the empirical equation.

(4) The normal-zone growth was investigated. The normal growth delayed since the heater was on and the subsequent propagation was relatively faster.

(5) The results contributed to the design of the conductor for the LHD poloidal coils.

References

[1] O. Motojima, Design and status of superconducting Large Helical Device, IEEE Trans. Magn. 27 (1991) 2214–2219.

[2] S. Mizumaki et al., Fabrication of the R&D Forced Flow Poloidal Coil (TOKI-PF), Proc. ITC-3, Toki, Japan (1991), to be published.

[3] PROPATH Group, A Program Package for Thermophysical Properties of Fluids, Version 7.1 (Corona Publishing, Japan, 1990).

[4] R.H.F. Pao, Fluid Mechanics (Wiley, New York, 1961) pp. 235–286.

[5] E. Tada et al., Thermal performance results of the Nb–Ti demo poloidal coils (DPC-U1, U2), Proc. Int. Conf. on Magnet Technology, Tsukuba, Japan (1989) pp. 830–834.

[6] K. Shibata et al., Training behavior and acoustic emission of superconducting magnet, Adv. Cryog. Engrg. 29 (1984) 175–182.

[7] T. Mito et al., Voltage oscillations with wire movements in superconducting magnets, Proc. Int. Symp. on Flux Pinning and Electromagnetic Properties in Superconductors, Fukuoka, Japan (1985) pp. 187–190.

[8] J.W. Lue and J.R. Miller, Extended field operation of an internally cooled superconducting magnet, Proc. 9th Symp. on Engineering Problems on Fusion Research, New York, USA (1981) pp. 269–272.

[9] J.R. Miller, Empirical investigation of factors affecting the stability of cable-in-conduit superconductors, Cryogenics 25 (1985) 552–557.

[10] L. Dresner, The growth of normal zones in cable-in-conduit superconductors, Proc. 11th Symp. on Fusion Engineering, Philadelphia, USA (1983) pp. 2040–2043.

[11] Y. Wachi et al., Development of forced-cooled superconducting coil for Large Helical Device, IEEE Trans. Magn. 27 (1991) 2228–2231.

[12] T. Ando et al., Propagation velocity of the normal zone in a cable-in-conduit conductor, Adv. Cryog. Engrg. 35 (1990) 701–708.

Presented at MT-13
Victoria, Canada
September 20-24, 1993
OI-3

Stability Tests of the Nb-Ti Cable-in-Conduit Superconductor with Bare Strands for Demonstration of the Large Helical Device Poloidal Field Coils

K. Takahata, T. Mito, T. Satow, N. Yanagi, M. Sakamoto, S. Yamada, A. Nishimura, J. Yamamoto, O. Motojima
National Institute for Fusion Science, Oroshi-cho, Toki, Gifu 509-52, Japan

H. Ogata, T. Yoshida, M. Ono, H. Takano, S. Ioka
Toshiba Corporation, Chiyoda-ku, Tokyo 100, Japan

N. Aoki
Showa Electric Wire & Cable Co., Ltd, Kawasaki, Kanagawa 210, Japan

J. W. Lue
Oak Ridge National Laboratory, Oak Ridge, TN37831-8040

D. Kasao
Kyushu University, Fukuoka 812, Japan

Abstract—Stability and quench experiments of a Nb-Ti cable-in-conduit superconductor with bare strands have been carried out to determine the performance of the poloidal coil for the Large Helical Device (LHD). The conductor was formed into a double-pancake coil named IV-S and was mounted on TOKI-PF - a previously tested R&D coil. In excitation tests at 7.4~8.3K, the IV-S coil reached the critical currents without premature quenches. Stability tests at 7.5K indicated that the limiting current exceeds 20kA, which is the nominal operating current of the LHD poloidal coils. These results demonstrated that the stability of the chosen conductor with bare strands is high enough for the LHD.

I. Introduction

The Large Helical Device (LHD) is a heliotron type fusion experimental device and has been constructed since 1990 [1]. One of the special futures of the LHD is that all magnetic systems are superconducting. The LHD has a pair of helical coils and three pairs of poloidal coils. Inner vertical (IV) coils, which are the smallest pair in the poloidal coils, have been completed already. Inner shaping (IS) coils are now under construction. Outer vertical (OV) coils, of which diameter is 11.3 m, will start from 1994. Conductors of the IV and IS coils are Nb-Ti cable-in-conduit types as shown in Table I. Both conductors have almost the same specifications except for the copper ratio. As for the IS conductor, the Nb-Ti fraction of the strand was reduced because the maximum field is lower than the IV coil. In this paper, we deal with stability of the conductor used for the IV and IS coils.

Before the construction of the IV coil, some R&D's have been performed. We first made a demonstration coil named TOKI-PF [2], [3]. In the previous experiments of TOKI-PF, several problems were found out [4]. First the coil quenched before reaching the critical point and the training behaviors were observed. Second the limiting current was observed at 15 kA, which was lower than the expected value. We considered that the formvar coating on the strand surface had bad influence on the stability due to the low heat transfer and uneven current distribution. After the experiments, we decided to remove the insulation around the strands in order to improve the stability. We then constructed a double pancake coil with the improved conductor and named IV-S. The IV-S was energized together with TOKI-PF. In this paper, we make a comparison of stability between the TOKI-PF and IV-S coils. We also discuss about the stability of the IV conductors.

Table I
Principal specifications of the IV and IS conductors

Conductor	IV	IS (Design)
Type	Cable-in-conduit	Cable-in-conduit
Superconducting material	Nb-Ti	Nb-Ti
Conduit dimension	23.0 mmx27.6 mm	23.0 mmx27.6 mm
thickness	3.0 mm	3.0 mm
Void fraction	0.377	0.38
Strand diameter	0.762 mm	0.760 mm
Number of strands	486	486
Nb-Ti:Cu	1:2.69	1:3.52
Strand surface	Bare	Bare
Operating Current	20.8 kA	21.6 kA
Maximum Field	6.5 T	5.4 T
Operating temperature	4.5 K-4.8 K	4.5 K-4.8 K
pressure	<1.0 MPa	<1.0 MPa

Manuscript received September 20, 1993.

Table II

Comparison of the TOKI-PF and IV-S conductors

Conductor	TOKI-PF	IV-S
Type	Cable-in-conduit	Cable-in-conduit
Superconducting material	Nb-Ti	Nb-Ti
Conduit dimension	17.0 mmX22.5 mm	17.0 mmX22.5 mm
thickness	1.0 mm	1.0 mm
Void fraction	0.40	0.345
Strand diameter	0.673 mm	0.707 mm
Number of strands	486	486
Nb-Ti:Cu:Cu-Ni	1:1.65:0.4	1:2.54:0
Strand surface	Formvar coating(11μm)	Bare

Table III

Principal specifications of the TOKI-PF and IV-S coils

Coil	TOKI-PF	IV-S
Configuration	Two double pancakes	One double pancake
Inner radius	0.6 m	0.6 m
Outer radius	0.82 m	0.76 m
Height	0.11 m	0.052 m
Number of turns	40	16
Cooling method	Forced flow	Forced flow
Operating temperature	>4.5 K	>4.5 K
pressure	<1 MPa	<1 MPa
Number of cooling paths	4 paths	2 paths
Design mass flow rate	16 g/s (total)	10 g/s (total)
Cooling path length	45 mx4	34.5 mx2

II. Conductor and Coil Arrangement

Comparison of the TOKI-PF and IV-S conductors is summarized in Table II. The IV-S conductor was designed concentrating on the stability. The most important difference is the surface of the strands. We removed the formvar which was used on the strand surface for TOKI-PF coil. Moreover, we remove Cu-Ni in the strand to increase the copper ratio. The void fraction was also reduced by increasing the strand diameter in order to avoid strand movements. As for the conduit, both conductors have the same dimensions. Fig. 1 is the photograph of the cross-section of the IV-S conductor.

The conductor of 70 m was formed into a double-pancake and mounted on TOKI-PF. Specifications of the TOKI-PF and IV-S coils are listed in Table III. Both coils have the same inner radius of 0.6 m. The IV-S coil was attached to TOKI-PF truing up the center as shown in Fig. 2. The two coils were joined up in series and both ends were connected to current leads. Dotted lines in Fig. 3 indicate a current path. Cooling paths are also indicated schematically in Fig. 3. The coils consist of six parallel flow paths. Supercritical helium (SHE) flows from the inner turns to the outer turns with a pressure of 1 MPa or less. Design mass flow rates are 10 g/sec for IV-S and 16 g/sec for TOKI-PF.

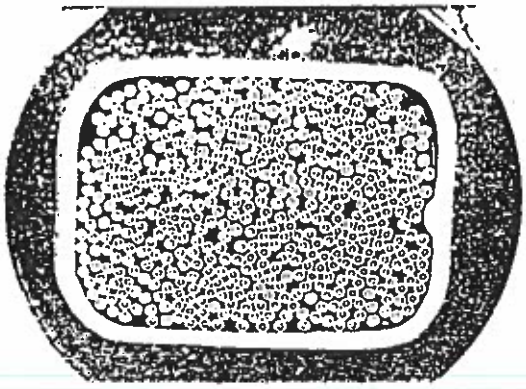

Fig. 1 Photograph of the cross-section of the IV-S conductor

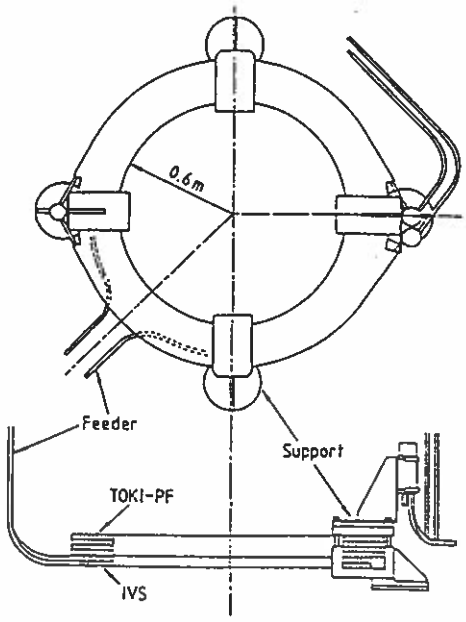

Fig. 2 Coil arrangement

Peak magnetic fields are 2.7T in IV-S and 2.8 T in TOKI-PF with the current of 20 kA. These fields are lower compared with the IV and IS coils of LHD; a maximum field of IV is 6.5 T at 20.8 kA as shown in Table I. Therefore, we performed the experiments at higher temperature, 7.4~8.3 K, to bring a load close to the IV and IS coils.

II. Experimental Procedure

In the experiments, we concentrated on the following two properties; one is operating limits and the other is the stability margin. Fig. 3 shows instrumentations required for the experiments. Resistive heaters (RH1 and RH2) were attached on the inlet pipes for the both coils to increase the SHE temperature. Inductive heaters (IH1~IH6) were wound

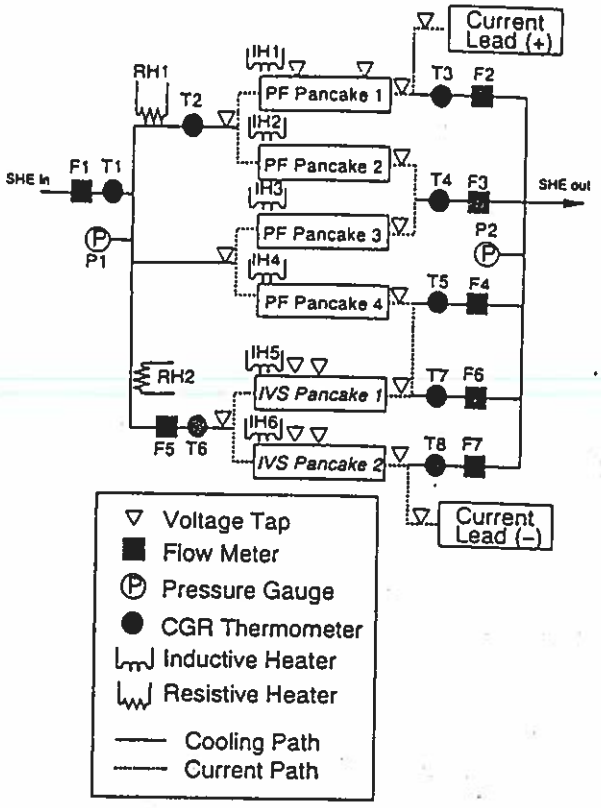

Fig. 3 Instrumentations of the experiment

around the conductor near the SHE inlet in order to measure the stability margin. Flow meters (F), carbon-glass-resistor (CGR) thermometers (T) and pressure gauges (P) were installed on the inlet and outlet pipes. A normal zone was detected by voltage taps.

Both current and temperature limits were measured with regard to the operating limits. First we measured the quench current under the condition that the temperature was constant, from 4.5 K to 8.1 K. Second we measured a temperature at which the coil just quenched under the condition that the current was constant. The temperature was controlled by the resistive heaters. By comparing the two results, we could estimate the effect of mechanical disturbances which may appear when ramping up the current. The temperature limit is not affected by the disturbances because the electro-magnetic force is constant. Therefore, the limit may correspond to the current sharing temperature. The quench current does not necessarily agree with the critical current because of the disturbances.

The stability margin was measured by the inductive heaters with a length of 0.1 m and 200 turns. The power supply consists of silicon controlled rectifiers, a capacitor bank of 0.4 mF and 1 kV. In the experiments, current discharges were obtained with an oscillation frequency of 500 Hz and a decay time constant of 5 msec. It is usually difficult to calibrate an input energy. We, then, apply a calorimetric method. Fig. 4 shows a typical time variation of

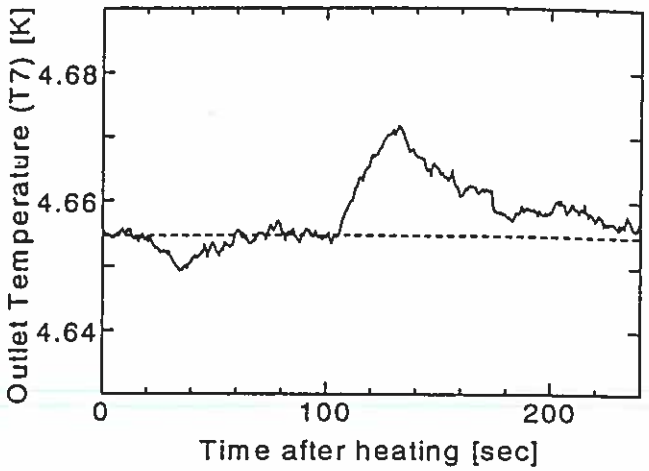

Fig. 4 Time variation of the outlet temperature (T7) after heating by the inductive heater (IH5)

the outlet temperature (T7) after heating by the heater (IH5). At that time, the capacitor bank was charged up to 520 V. The temperature increased from the initial temperature, 4.655 K after 100 sec. If assuming that the heat did not run away to the neighboring layer, the input energy can be calculated from the integration of the increase of helium enthalpy.

The margin of IV-S was measured at the temperature of 4.5 K and 7.5 K with the pressure of 1.0 MPa and 0.5 MPa. First the coils were energized to a certain current. Then the conductor was heated by the inductive heater (IH5). If the coil did not quench, the capacitor bank was charged up to a slightly higher voltage and then discharged. The heating was repeated with the sufficient intervals until the coil quenched.

III. Results

A. Operating Limits

In the beginning of the experiments, the current limits were measured at various temperatures. The pressure of SHE was 1.0 MPa and current sweep rate was 50 A/sec for all excitations. Fig. 5 and Fig. 6 show the quench points on the load line for the TOKI-PF and IV-S coils, respectively. In the figures, critical currents ($I_{c,cal}$) extrapolated from 4.2 K single strand short sample measurements up to 7 T are also presented. The TOKI-PF coil quenched at 4.5 K, 22.5 kA and 3.15 T, which was 45 % of the critical point. In the previous tests, the quench current was also measured. The results are shown in Fig. 5 as a single operation. The quench current was 26.3 kA at 2.83 T. It should be noted that the products of the quench current and the magnetic field are almost the same between the single and the combined operation. That indicates that the quench origin lies in the electro-magnetic force. The quench current at 7.4 K was 14.9 kA, 65 % of the critical current.

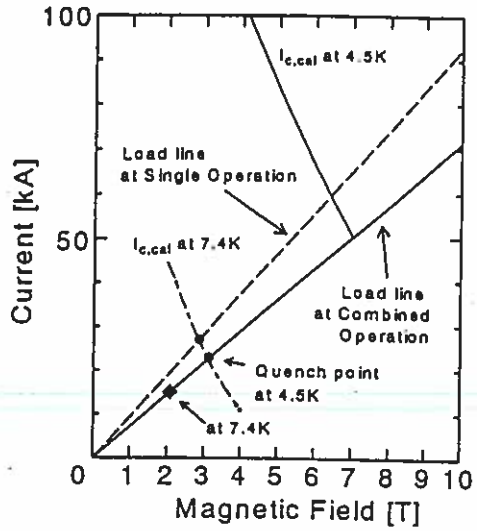

Fig. 5 Quench currents of the TOKI-PF coil on the load line

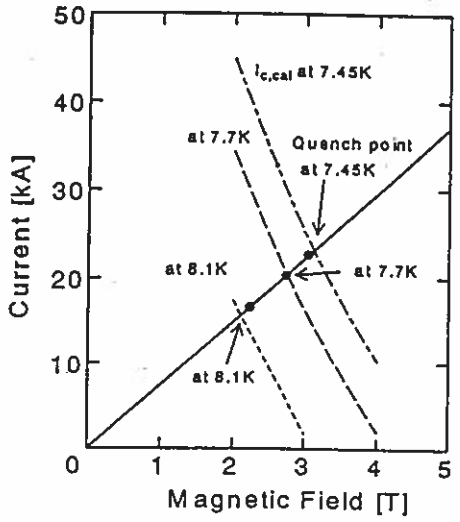

Fig. 6 Quench currents of the IV-S coil on the load line

On the other hand, the IV-S coil quenched at almost the same current as the critical current, 16.6 kA at 8.1 K, 20.3 kA at 7.7 K and 22.6 kA at 7.45 K. We could not measure the quench current under 7.45 K because the TOKI-PF coil quenched before IV-S. The differences between the quench and the calculated critical current may be caused by the error of the extrapolation. The temperature limits were also measured in order to clarify the critical points. The temperature limit must correspond to the current sharing temperature because the limit was not affected by the wire movement. The results are summarized in Fig. 7. The closed and the open circles indicate the current and the temperature limits, respectively. Both limits lie in the same line as is evident from the figure. Then it is concluded that the IV-S coil can be energized up to the critical point without any

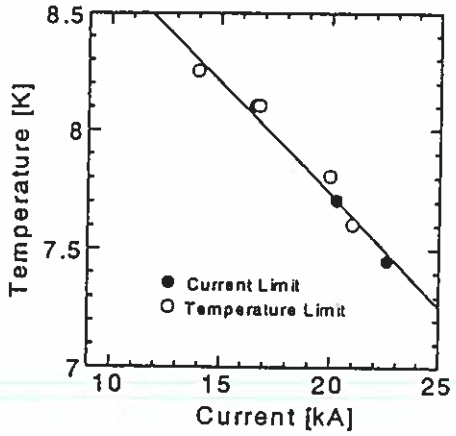

Fig. 7 Comparison between the current and temperature limits

degradation.

The results of the limit measurements confirmed that the IV-S coil has much higher performances than TOKI-PF. There are two reasons for this improvement of the performance. One is the decrease of mechanical disturbances due to the strand movements since the void fraction was reduced for the IV-S coil. The other is the improvement of the stability margin due to the removal of the insulation on the strand surface. We performed the stability margin measurements in order to confirm the above reasons.

B. Stability Margin

Fig. 8 shows the results of the stability margin measurements at 4.5 K. As for the TOKI-PF coil, the data obtained in the previous tests are presented. The solid and the dashed line shows the helium enthalpy calculated by the following equation on the IV-S and the TOKI-PF coil, respectively.

$$\Delta H = (1-f)/f \int_{T_b}^{T_{sh}} \rho_{He} C_p \, dT \qquad (1)$$

where f is the volume fraction of the strands inside the cable space, T_b and T_{sh} are the bath and the current sharing temperature, respectively, ρ_{He} is the helium density, and C_p is the specific heat at constant pressure of helium. The limiting current [5], [6] was observed at 15 kA on the TOKI-PF coil. The margin was below 10^5 J/m^3 when the current was larger than 15 kA, and about 4×10^4 J/m^3 at the quench current, 26.3 kA. The margin of IV-S was measured at only 21 kA, which is the nominal current of the IV and IS coils. The coil did not quench up to 8×10^5 J/m^3,and we could not quench it because of limitations of the power supply. It was, however, evident that the margin stayed in the upper stability region, and the limiting current was higher than 21 kA. It is concluded that the stability was improved by removing the insulation on the strand surface.

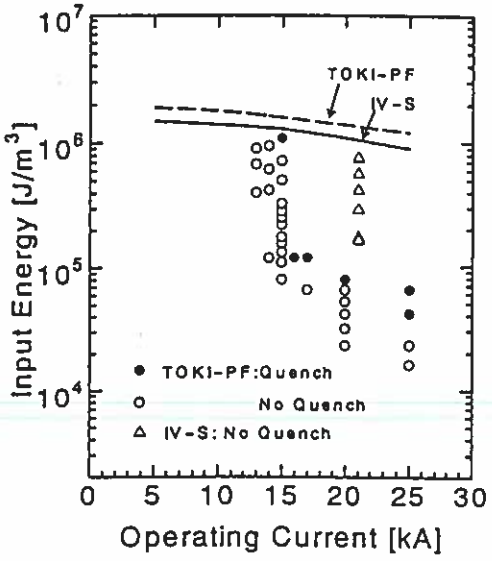

Fig. 8 Results of the stability margin measurements at 4.5K.

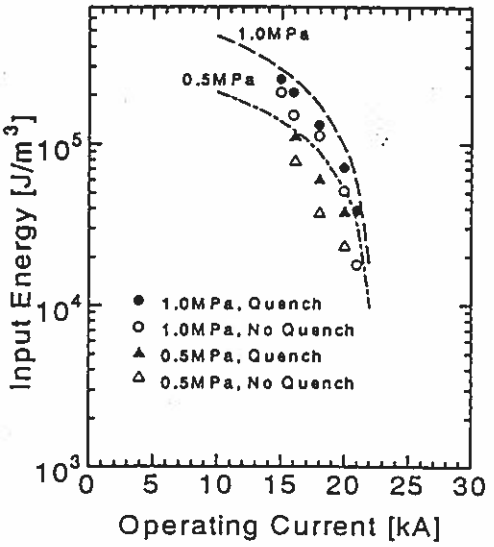

Fig. 9 Results of the stability margin measurements at 7.5K on the IV-S coil.

The margin of IV-S was then measured at 7.5 K at a pressure of 1.0 MPa or 0.5 MPa. The results are shown in Fig. 9. The dashed and the dash-dotted line indicates the available helium enthalpy calculated by (1). The margins were all very close to the calculated available enthalpy in the both cases of 1.0 MPa and 0.5 MPa. Thus the conductor stayed in the upper stability region up to 21 kA, which was about 94 % of the critical current. It can be concluded that the limiting current is higher than the critical current under the present conditions. It can also be inferred that energy deposition due to strand movements must be less than 3×10^4 J/m^3, the measured stability margin at 21 kA, because the coil did not quench up to 21 kA. The inferential energy deposition was lower than TOKI-PF, 4×10^4 J/m^3. The reason of this may be caused by reducing the void fraction.

If assuming that the dimensions are the same, the limiting current is proportional to $(T_c-T_b)^{1/2}\rho^{-1/2}$, where T_c and T_b are the critical and the bath temperature, and ρ is the resistivity of copper [5]-[7]. As for IV-S, the limiting current was higher than 21 kA at 7.5 K. In this condition, $(T_c-T_b)^{1/2}\rho^{-1/2}$ is estimated to be 5.8×10^4. On the other hand, $(T_c-T_b)^{1/2}\rho^{-1/2}$ is 7.4×10^4 at the nominal condition of the IV coil, B=6.5 T, I=20.8 kA and $\rho=4\times10^{-10}$ Ωm. This value is 1.3 times higher than IV-S. Thus it can be expected that the limiting current of the IV coil is higher than the nominal operating current.

IV. Conclusions

The Nb-Ti cable-in-conduit superconductor with bare strands was developed, and stability and quench experiments were carried out in the form of a double-pancake to demonstrate the performance of the poloidal field coil for the LHD. A summary of the results is shown below.

(1) The quench current and the stability margin were improved by removing the insulation of strand surfaces.

(2) The energy deposit due to strand movements was reduced by the reduction of the void fraction.

(3) It can be expected from the stability margin measurements that the limiting current is higher than the nominal current for the IV and IS coils.

References

[1] T. Satow, et al., "Present status of design and manufacture of the superconducting magnets for the Large Helical Device," IEEE Trans. on Appl. Supercon., Vol. 3, pp. 365-368, March 1993.

[2] K. Takahata, et al., "Design and fabrication of forced-flow coils as an R&D program for Large Helical Device," IEEE Trans. on Magn., Vol. 27, pp. 2353-2356, March 1991.

[3] S. Mizumaki, et al., "Fabrication of the R&D forced-flow poloidal coil (TOKI-PF)," Fusion Engineering Design, Vol. 20, pp. 153-159, 1993.

[4] K. Takahata, et al., "Experimental results of the R&D forced-flow poloidal coil (TOKI-PF)," Fusion Engineering Design, Vol. 20, pp. 161-166, 1993.

[5] Lawrence Dresner, "Parametric study of the stability margin of cable-in-conduit superconductors: Theory," IEEE Trans. on Magn., Vol. 17, pp. 753-756, January 1981.

[6] J. W .Lue and J. R .Miller, "Parametric study of the stability margin of cable-in-conduit superconductors: Experiment," IEEE Trans. on Magn., Vol. 17, pp. 757-760, January 1981.

[7] T. Ando, M. Nishi and S. Shimamoto, "Measurements of the stability margin of a Nb_3Sn cable-in-conduit conductor," IEEE Trans. on Magn., Vol. 25, pp. 2386-2389, March 1988.

STABILITY OF CABLE-IN-CONDUIT SUPERCONDUCTORS FOR LARGE HELICAL DEVICE

K. Takahata, T. Mito, T. Satow, N. Yanagi, M. Sakamoto,
S. Yamada, A. Nishimura, J. Yamamoto, O. Motojima
National Institute for Fusion Science, Nagoya, 464-01, Japan
S. Mizumaki, K. Nakamoto, T. Uchida, Y. Wachi, M. Shimada, S. Itoh, S. Ioka
Toshiba Corporation, Chiyoda-ku, Tokyo 100, Japan

Abstract--The stability of cable-in-conduit superconductors has been experimentally investigated as a program of poloidal field coils for the Large Helical Device (LHD) project. On the excitation tests for the demonstration coil (TOKI-PF), we had found several problems on the stability of a cable-in-conduit conductor; strand movements, current distribution and current transition among the strands. Consequently, a new conductor was designed and fabricated focused on the stability. As a result of a zero-dimensional stability analysis, it was found that the conductor has high stability margin, $5\times10^5 J/m^3$, at the design condition of 20.8 kA and 6.5 T. Current transfer performance after partial quenching has been investigated by a short sample test. In this paper, effects of the current transfer among the strands on the conductor stability will also be discussed.

I. INTRODUCTION

Large Helical Device (LHD) is a heliotron/torsatron type fusion experimental device and its construction is progressing as a 7 year project which began in 1990. In 1991, we started the construction of one of the poloidal field coils, named Inner Vertical Coil (IV-coil) [1]. From the research and development programs, we decided to design the conductor focused on reliability and stability. In this paper, we deal with stability of the conductor used for the IV-coil.

Stability of cable-in-conduit conductors has been theoretically studied by using zero- and/or one- dimensional models [2,3]. Here we include the effects of normal propagation and current transfer in the transverse direction of a conductor. In the excitation tests of the demonstration coil (TOKI-PF), the conductor was found to be unexpectedly unstable [4]. In this coil, the strands were insulated with formvar of 11 μm thickness in order to reduce the coupling losses. We confirm that there are some problems concerning the insulation. First, the formvar insulation reduces the heat transfer coefficient effectively. Second, rapid commutation of current may lower the stability. The quench of a multi-strand cable may originate from the normal transition of some portions of the strands. Vysotsky et al. pointed out that the current transfer from a strand with the normal zone to the adjacent strand occurred rapidly when using insulation or high resistive matrices, and the quench current of the adjacent strand could not reach the DC critical one [5].

In the experiment presented here, the current transfer in the transverse direction was studied using a short sample of the conductor for the IV-coil. A partial normal zone was generated by a resistive heater instead of an inductive heater and the current distribution was monitored by pick-up coils.

II. CONDUCTOR DESIGN

Main parameters of the new conductor are listed in Table 1. In order to improve the stability of the conductor, we decided to use neither resistive layers on the strand surface nor CuNi layers inside the strands. Cu/NbTi ratio and critical/operating current ratio are set to be 2.7 and 3, respectively. Copper resistivity was reduced as small as possible. The critical current measured with a short sample is shown in Fig. 1. The open circles are the measured values and the dashed line is the calculated one by using the critical current of the strand. The measured values agreed with the calculated one, which confirms no damage of the strands. The critical current was extrapolated to be 62 kA at 6.5 T which is just three times as large as the operating one. We designed these parameters in consideration of the stability margin. Figure 2 shows the calculated margin. In the analyses, a zero-dimensional model proposed by L. Bottura and J. V. Minervini [6] was applied. Magnetic field is proportional to the operating current, I_{op}. The results indicate that the margin decreases rapidly when the operating current exceeds 20 kA. The limiting current was, therefore, estimated to be approximately 20 kA. The margin, however, keeps rather high value, 5×10^5 J/m^3, at the designed point.

Table 1. Parameters of conductor for IV-coil.
All dimensions are measured values.

Conduit Dimension	22.9 mm×27.7 mm
Thickness	2.9 mm
Material	SUS316L
Void fraction	38 %
Strand Diameter	0.767 mm
Configuration	$3^4\times6$
Cabling pitch: 1st	60 mm
2nd	95 mm
3rd	145 mm
4th	225 mm
5th	408 mm
Strand Composition	1:2.66 (NbTi:Cu)
Resistivity of Copper	4×10^{-10} Ω m at 6.5 T
Filament Diameter	15 μm

Manuscript received August 24, 1992

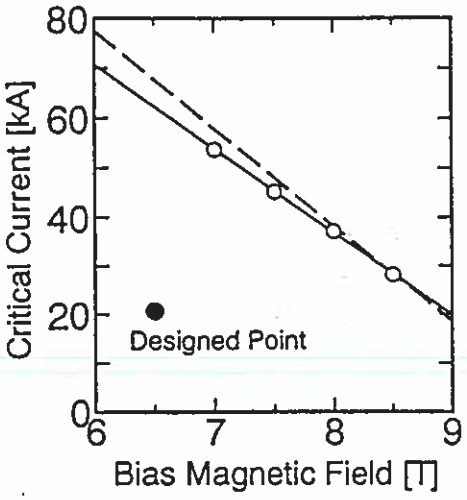

Figure 1. Measured critical current of the conductor. The dashed line is the calculated value using the critical current of the strand.

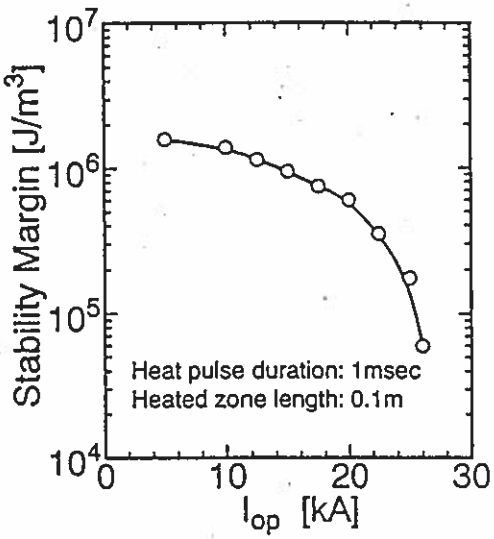

Figure 2. Calculated stability margin. Magnetic field is proportional to the operating current, I_{op}, with a factor of 3.1×10^4 T/A.

III. EXPERIMENTAL SETUP

Experiments were carried out by using a large-scale conductor test facility in which a split coil generates the background magnetic field up to 9 T. A power supply has a capacity of 75 kA. A pair of test conductors was inserted into a bore of the split coil. Length of each conductor was 1.2 m except joint parts. The end of each conductor was jointed to the current leads and the opposite side was soldered each other. In the joint parts, the conduit was removed and the strands were unbound. In this experiment, we used liquid helium (4.58 K) for the coolant instead of the supercritical helium, since the electromagnetic features of the cable do not depend on the coolant condition. The arrangement of a heater and pickup coils is schematically illustrated in Fig. 3. The resistive foil heater of 350 Ω was attached to about ten strands. The heater current pulse had a rectangular shape with a duration of 1 sec and generated heat up to 5 J. Eight pickup coils with 200 turns surrounded the conductor to detect the magnetic field produced by the transport current. Output signals of the coils were integrated to give the magnetic field change.

Figure 4 shows the longitudinal locations of a heater, pickup coils and voltage taps. The heater and the eight coils (PC09~PC16) were located at the center of the background split coil. A pair of eight pickup coils (PC01~PC08 and PC17~PC24) was similarly set at the distance of 200 mm from the center. The distance corresponds to 1/2 of the 5th cabling pitch and the positions of strands then rotate almost 180 degrees. The voltage taps (E_b~E_f) were attached on the conduit at intervals of 68 mm.

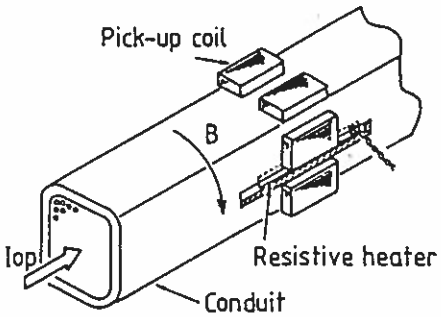

Figure 3. Arrangement of a heater and pickup coils

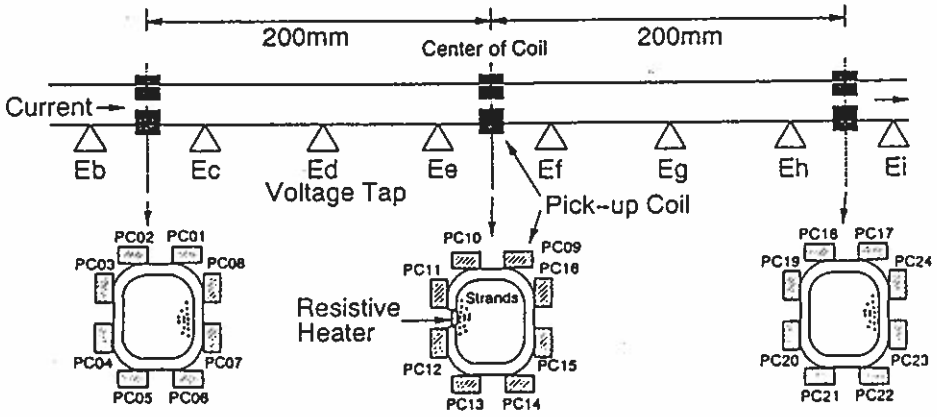

Figure 4. Locations of a heater, pickup coils and voltage taps.

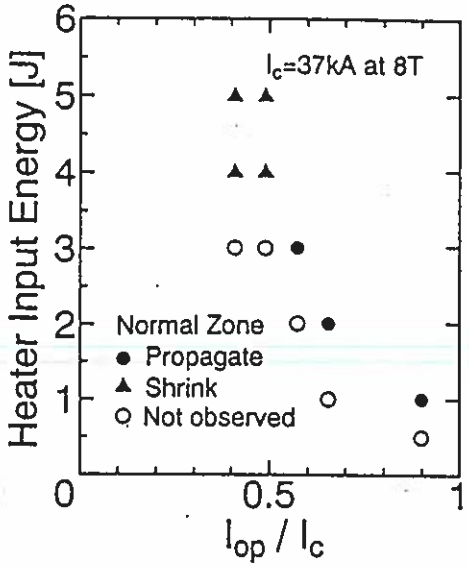

Figure 5. Plots of the minimum heater input energy required to initiate the normal transition versus the operating/critical current ratio, I_{op}/I_c.

IV. RESULTS AND DISCUSSION

Figure 5 shows the plots of the minimum energy required to initiate the normal transition versus the operating/critical current ratio, I_{op}/I_c. Though the normal zone propagated for $I_{op}/I_c>0.5$, it shrank for $I_{op}/I_c<0.5$. It should be noted that the operating current of $I_{op}/I_c=0.5$ corresponds to the recovery current which is observed for pool-boiling type conductor.

Figure 6 shows the time evolution of voltages and field changes, ΔB, at 18.2 kA ($I_{op}/I_c=0.49$) where the normal zone shrank. When the voltage generation was initiated, the field at the positions of PC07, PC11 and PC24 decreased, since the field produced by the initial transported current has a positive sign. These pickup coils were located near the strands attached to the heater (see Fig. 4). So, the field decrease indicates that the current in the strands with the normal zone was transferred to adjacent strands which were far from these pickup coils. Though the heater input continued for 1 sec, the voltage vanished in about 0.2 sec. This can be explained as follows: the current with the normal zone dropped down to nearly zero and then the voltage vanished. Although the current of the adjacent strands increased, they were still superconducting. The data also show that ΔB saturated after the vanish of the voltage, which indicates that the distribution of the transport current has been changed due to the generation of the partial normal zone.

Figure 7 shows the time evolution where the normal zone propagated at 21.3 kA ($I_{op}/I_c=0.57$). The change of ΔB seems to be composed of two phenomena. ΔB for the initial 0.08 sec (period I in the figure) was almost similar to the previous data at 18.2 kA. ΔB at PC11 decreased and then saturated. This means that only the strands near the heater quenched in the period I. In the subsequent period (II in the figure), ΔB at PC11 and PC13 decreased and the others increased along with the increase of the voltage signals. The distribution of ΔB indicates that the current was transferred in the transverse direction.

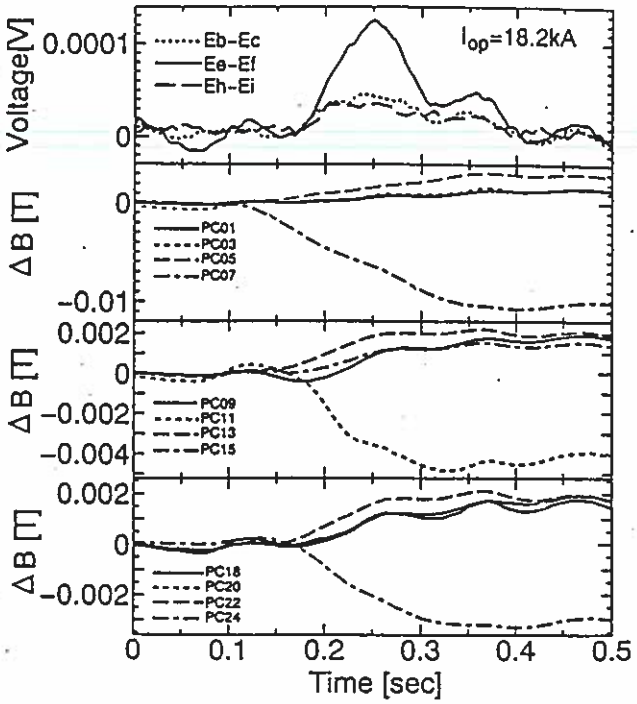

Figure 6. Time evolution of voltages and field changes, ΔB. The normal zone shrank at 18.2 kA and 8 T. Heater was on from -0.1 sec to 0.9 sec.

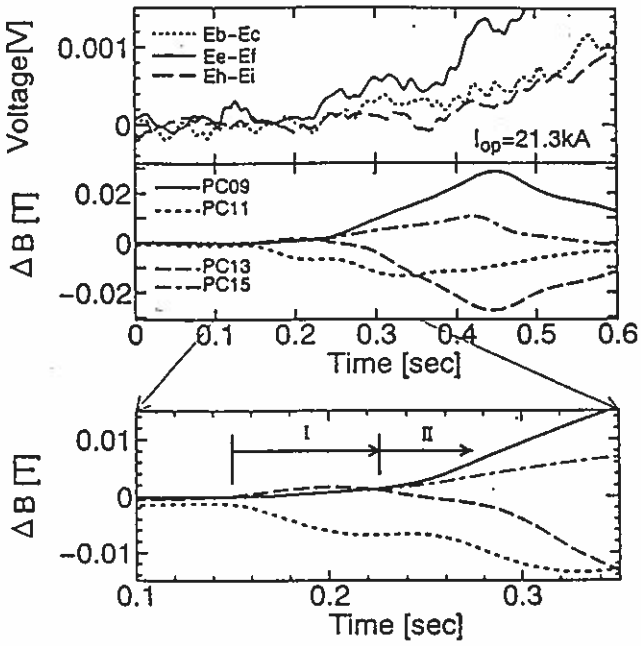

Figure 7. Time evolution of voltages and field changes, ΔB. The normal zone propagated at 21.3 kA and 8 T. Heater was on from -0.1 sec to 0.9 sec.

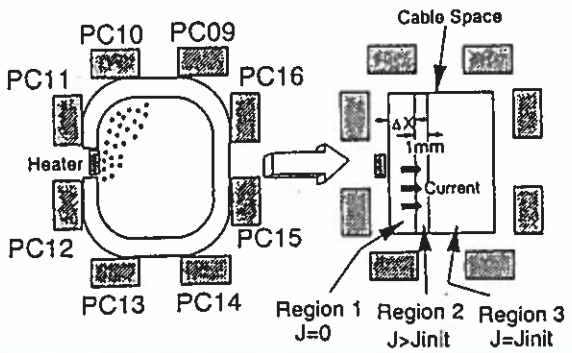

Figure 8. A Model for calculating the field changes due to the transverse transfer of the transport current.

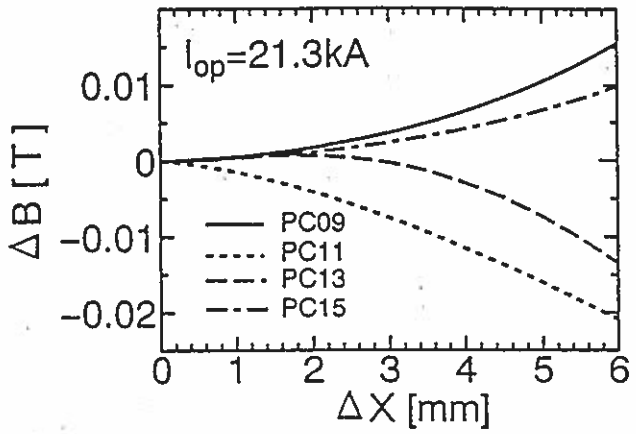

Figure 9. Calculated results of the field change due to the current transfer. ΔX is defined in Fig. 8.

We calculated ΔB by using a simplified model as shown in Fig. 8 in order to confirm the current transfer process. In this model, the current in the region 1 with the width of ΔX drops down to zero and this current is added to the region 2 of 1 mm width. The width of 1 mm simulates a row of strands. The current density in the region 3 is assumed to be constant. The calculated results are shown in Fig. 9. ΔB at PC11 decreases and ΔB at PC09 and PC15 increase with increasing ΔX. ΔB at PC13 decreases as ΔX>2 mm. These tendencies were consistent with the experimental results. In period I, ΔX was evaluated to be 2~3 mm. In Fig. 7, all ΔB's approached zero again from 0.45 sec, which indicates that the current density became uniform since all the strands turned into normal states.

It should be noted that the stability boundary appeared at I_{op}/I_c~0.5. At 21.3 kA, the normal propagation started after the commutation. The reason may be that the current in the adjacent strands increased and finally exceeded the critical current. The strands over the critical current must have quenched in a long region if the magnetic field is constant. If considering a two-strand cable, it is clear that the stability boundary is I_{op}/I_c=0.5. In the experiment, the phenomenon similar to the two-strand system may occurred. Vysotsky et al. reported that quench current of the adjacent strand cannot reach the critical one if the duration of commutation is rapid, the order of 1 msec [5]. The duration was, however, about 100 msec in our sample. The joint resistance between strands may be effectively reduced because of no insulation of strands.

The experimental results suggest that the critical current should be more than twice as large as the operating one in regard to a cable-in-conduit conductor. The IV-coil has the critical current of three times. Therefore, we expect high stability in the operating condition.

V. CONCLUSIONS

Stability of the conductor for LHD poloidal coils was experimentally investigated concentrating on partial quenching using a resistive heater installed in the conduit. The summary of the results is shown below.

(1) Propagation of normal zone was observed when the operating/critical current ratio exceeded 0.5. In the case of I_{op}/I_c<0.5, the current in the quenching strand dropped down to zero and the adjacent strand could carry the superconducting current. In the case of I_{op}/I_c>0.5, the current in the adjacent strand seemed to exceed the critical one and then the transverse and longitudinal propagation of the normal zone progressed.

(2) The experimental results showed that it took approximately 100 msec to commutate the current fully from the quenching strand to the adjacent one. This duration was much larger than Vysotsky's observations, which may be related to no insulation of strands.

(3) In the actual design of IV-coil, the operating/critical current ratio is set to be 0.33. High stability margin is, therefore, expected in regard to the partial quenching.

REFERENCES

[1] T. Satow et al., "Present status of design and manufacture of the superconducting magnets for Large Helical Device," this conference.

[2] L. Dresner, "Parametric study of the stability margin of cable-in-conduit superconductor: theory," IEEE Trans. on Magn., Vol. MAG-17, pp. 753-756, January 1981.

[3] T. Ando, M. Nishi and S. Shimamoto, "Measurements of the stability margin of a Nb3Sn cable-in-conduit conductor," IEEE Trans. on Magn., Vol. 25, pp. 2386-2389, March 1989.

[4] T. Takahata et al., "Experimental results of the R&D forced-flow poloidal coil (TOKI-PF)," to be published in Fusion Engineering and Design.

[5] V. S. Vysotsky, V. N. Tsikhon and G. B. J. Mulder, "Quench development in superconducting cable having insulated strands with high resistive matrix (part 1, experiment)," IEEE Trans. on Magn., Vol. 28, pp. 735-738, January 1992.

[6] L. Bottura and J. V. Minervini, "Modelling of dual stability in a cable-in-conduit conductor," IEEE Trans. on Magn., Vol. 27, pp. 1900-1903, March 1991.

[7] T. Mito et al., "Short sample tests of full-scale superconducting conductors for Large Helical Device," IEEE Trans. on Magn., Vol. 28, pp. 214-217, January 1992.

PRESENT STATUS OF DESIGN AND MANUFACTURE OF THE SUPERCONDUCTING MAGNETS FOR THE LARGE HELICAL DEVICE

T. Satow, J. Yamamoto, K. Takahata, S. Imagawa, H. Tamura, N. Yanagi, T. Mito, A. Nishimura, S. Satoh, K. Yamazaki, H. Kaneko, H. Yonezu, H. Hayashi, M. Takeo, O. Motojima and LHD Design Group
National Institute for Fusion Science, Nagoya, 464-01, Japan

Abstract--The Large Helical Device is a nuclear fusion experimental device with superconducting magnets. Manufacture of the cryostat, the two inner vertical coils, and the helical-coil winding machine are now being carried out. Designs for constructing two helical coils and two other pairs of poloidal coils are being carried on. The outside diameter of the torus-shaped cryostat is 13.5 m. The helical coils have a magnetic energy of 1.6 GJ and an overall current density of 53 A/mm^2 in Phase II. Its rated current is 13.0 kA in Phase I, and the maximum magnetic field in the helical coil winding in Phase I is calculated to be 6.9 T. Three pairs of poloidal coils are cooled by forced-flow supercritical helium because of the requirement of no metal coil vessel. The rated current of one inner vertical (IV) poloidal coil is 20.8 kA, and its stored energy is 80 MJ. The maximum magnetic field of the two IV coils is calculated to be 5.8 T. The type of superconductor for the IV coils is a cable-in-conduit conductor.

I. INTRODUCTION

The Large Helical Device (LHD)[1,2] is a nuclear fusion experimental device having two superconducting helical coils, three pairs of superconducting poloidal coils, cryogenic supporting structures, and a torus-shaped cryostat.

We have two operational stages for the LHD, Phase I and Phase II. A seven-year construction project, Phase I, started in 1990. The key parameter in Phase I is a central plasma field of 3 T. After experimental plasma research in Phase I, the next construction program, Phase II, is expected to begin, and the field will be enhanced up to 4 T. Enhancement of the helical field is planned to be obtained by changing pool-boiling liquid-helium cooling of the helical coils with Nb-Ti superconductors in Phase-I into superfluid-helium cooling in Phase II project.

The poloidal coils are designed and will be constructed in Phase I according to specifications of Phase II.

Two inner vertical (IV) coils, a lower part of the cryostat, and the winding machine for helical coils are under construction in summer 1992.

II. GENERAL DESCRIPTIONS OF THE SUPERCONDUCTING MAGNETS FOR THE LHD

Table 1 shows the major parameters of the helical coils and the poloidal coils for the LHD in both Phase I and Phase II operation. A magnetic energy of 1.6 GJ will be stored in the helical coils in Phase II. This maximum value has not been obtained so far. Furthermore, extremely high overall current densities, such as 40 and 53 A/mm^2 in Phase I and Phase II, respectively, must be attained for the requirement of plasma confinement.

Manuscript received August 24, 1992

The maximum magnetic fields in the helical coil winding in Phase I and Phase II were calculated to be 6.9 and 9.2 T, respectively. Nb-Ti was adopted as the superconductor for the helical coils. They are cooled by pool-boiling liquid helium in Phase I, but superfluid-helium cooling is indispensable in Phase II.

Figure 1 shows an outside view and cross section of the Large Helical Device. It consists of a plasma vacuum vessel, two superconducting helical coils, three pairs of superconducting poloidal coils, cryogenic supporting structures, and a torus-shaped cryostat.

The helical coils must be operated so as to generate constant magnetic fields during plasma experiments in both Phase I and Phase II. The poloidal coils must also be operated in the steady-state mode in Phase I, but the poloidal coil currents in Phase II will be varied for 5 s at intervals of 5 min. If any superconducting coil becomes quenched, all coils are assumed to be discharged with the same time constant of about 20 s.

Table 1 Major parameters of the helical coils and the poloidal coils for the LHD in both Phase I and Phase II project

	Phase I	Phase II
HELICAL COILS		
Major Radius	3.9 m	
Minor Radius	0.975 m	
Bath Temperature	4.2～4.4 K	～1.8 K
Central Magnetic Field	3 T	4 T
Magnetomotive Force	5.85MA×	7.80MA×2coils
Overall Current Density	～40 A/mm^2	～53 A/mm^2
Magnetic Stored Energy	0.9 GJ	1.6 GJ
POLOIDAL COILS		
OV Coil		
Position	(R=5.55 m, Z=±1.55 m)	
Magnetomotive Force	-4.5 MA×2coils	
Magnetic Stored Energy	0.60 GJ	
IS Coil		
Position	(2.82 m, ±2.00 m)	
Magnetomotive Force	-4.5 MA×2coils	
Magnetic Stored Energy	0.24 GJ	
IV Coil		
Position	(1.80 m, ±0.80 m)	
Magnetomotive Force	5.0 MA×2coils	
Magnetic Stored Energy	0.18 GJ	
Total Stored Energy	0.68 GJ	
Total Stored Energy when the Helical Coils and the Poloidal Coils are operated.	1.1 GJ	1.6 GJ

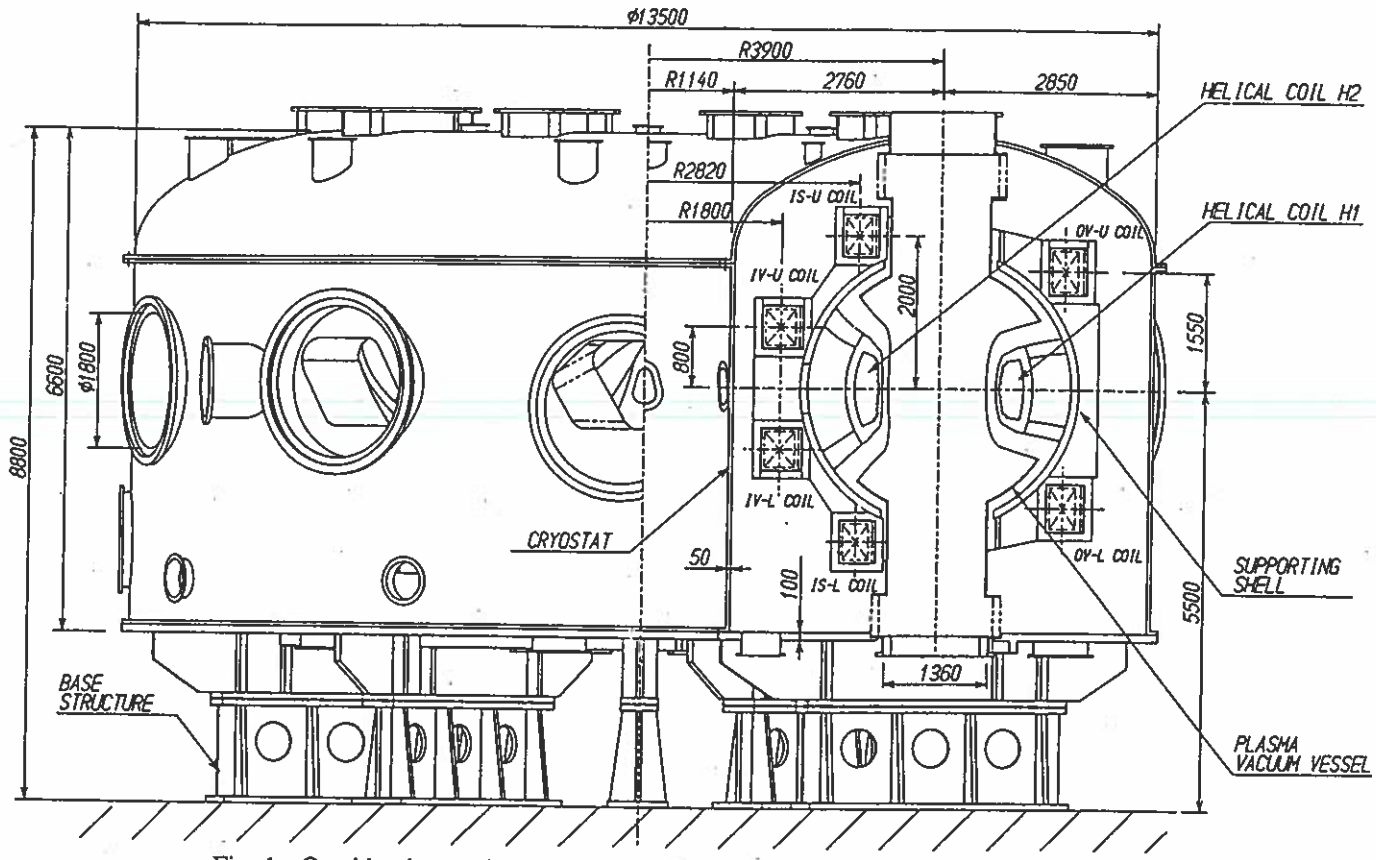

Fig. 1 Outside view and cross section of the Large Helical Device

III. CRYOSTAT AND CRYOGENIC SUPPORTING STRUCTURES

A. General

The outside diameter of the torus-shaped cryostat is 13.5 m. Its total height including base structures is 8.8 m. The cryostat consists of four cryostat vacuum vessels (a flat bottom section, an inside cylinder section, an outside cylinder section, and a curved top section), liquid-nitrogen-temperature thermal shields with multilayer insulators, cryogenic piping, nine pairs of current leads, their cryogenic ports, ten cryogenic supporting posts, forty room-temperature ports extended from the plasma vacuum vessel, etc.

B. Cryostat Vacuum Vessels and Base Structures

The bottom section and the top section of the cryostat each have ten room-temperature ports. The outside cylinder section has fourteen ports, and the inside cylinder section has six ports. The thicknesses of the flat bottom section and the other sections are 100 and 50 mm, respectively. They are made of 304 stainless steel equivalent. The total deformation of the cryostat vacuum vessel due to evacuation was calculated to be less than 2 mm in the vertical direction. The maximum stress on the vessel walls is no more than 80 MPa.

The base structures are made of 14 wt% Mn steel. Electrical insulators will be set up between them and the radial supporting ribs welded under the flat bottom section.

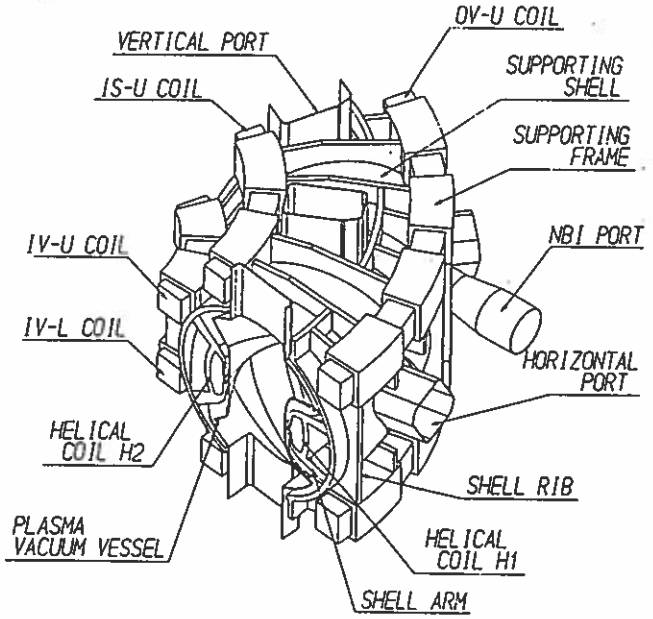

Fig. 2 Outside view of the cryogenic supporting structures

C. Cryogenic Supporting Structures

The cryogenic supporting structures are composed of shell arms, a supporting shell, shell ribs, and poloidal-coil supporting frames as shown in Fig. 2. The major feature of the supporting shell is that it has many large apertures for the room-temperature ports. Electromagnetic forces generated by the two helical coils are supported by the supporting shell through the shell arms.

The maximum deformation and stress on the 100 mm thick shell were calculated to be 3.6 mm and 370 MPa, respectively, in Phase II. The shell is made of highly-strengthened 316 stainless steel equivalent.

IV. SUPERCONDUCTING POLOIDAL COILS

A. General

Outlines of three pairs of poloidal coils are shown in Table 1 and Fig. 1. They are cooled by forced-flow supercritical helium, because a metal coil-vessel is necessary in a pool-boiling-cooled coil. The design for constructing the inner vertical poloidal coils (IV-L and IV-U coils) was carried out in accordance with specifications of Phase II, and the coils will be completed in 1993. The selection study of superconductors of other poloidal coils (inner shaping (IS) coils and outer vertical (OV) coils) is now ongoing. Their candidate conductors are a cable-in-conduit conductor and/or a hollow conductor.

The rated magnetomotive force of each IV coil is 5.0 MA, and its stored energy is 80 MJ. The combined stored energy of the two IV coils is 180 MJ. The maximum magnetic field of the two IV coils only was calculated to be 5.8 T, but that of the IV coils in a combined excitation with the helical coils and the other poloidal coils was 6.5 T.

B. Superconductor for the I V Coils

The type of superconductor for the IV coils is a cable-in-conduit conductor. The basic philosophy in selection of superconductor is as follows: Stability as d.c. superconducting magnet has top priority because the poloidal coils are operated in the steady-state mode in Phase I but in the very slow pulsed mode in Phase II. The maximum field changing rate in the IV coil winding is only 2.2 T / 5 s in Phase II operation. It is much slower than that of the poloidal coils of a tokamak system.

Consequently, a simple Nb-Ti and Cu monolithic conductor was chosen to increase stability as a superconducting strand of the IV coil. There is no Cu-Ni matrix. Its Cu / Nb-Ti ratio and critical current - operating current ratio (I_C / I_{OP}) were decided by the application of a stability theory of a tight-wound superconducting magnet [3].

A cross section of a fabricated strand is shown in Fig. 3. It has a diameter of 0.76 mm. The Cu / Nb-Ti ratio of the strand is 2.7. Short sample characteristics of several strands and two cable-in-conduit conductors were measured [4]. The strand has about three times the ratio I_C / I_{OP} at 4.58 K as designed. A group of Nb-Ti filaments is placed nearer by the center of the strand as possible of fabrication. No insulation is done on surface of a strand, so that the normal current flowing in one strand at quenching can easily transfer to other neighboring strands.

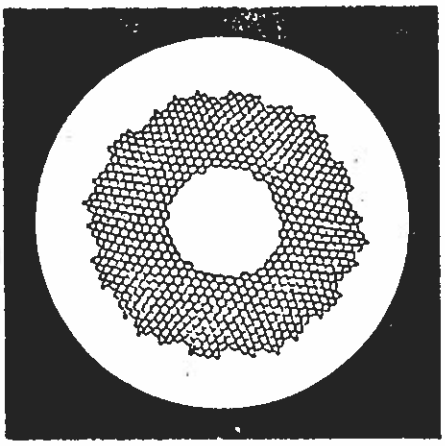

Fig. 3 Photograph of a cross section of a fabricated strand

The superconducting cable in a conduit consists of $3^4 \times 6$ strands twisted in the same right direction. The outer size of the conduit is 23.0 by 27.6 mm. The 316L stainless steel conduit has a thickness of 3 mm. It can support the hoop stress due to the IV coil itself.

C. I V Coil Winding

The type of IV coil winding is double-pancake. The number of double-pancakes is eight, and the number of turns per single-pancake is 15. The IV coil has an inner winding diameter of 1.44 m, an outer winding diameter of 2.16 m, and a height of 0.47 m.

The design characteristics of the IV coils are shown in Fig. 4. The rated current of the IV coils is 20.8 kA in Phase II. Short sample critical current curve is drawn by using the measured values. The overall current density of the IV coil is 30 A/mm^2 at the rated point.

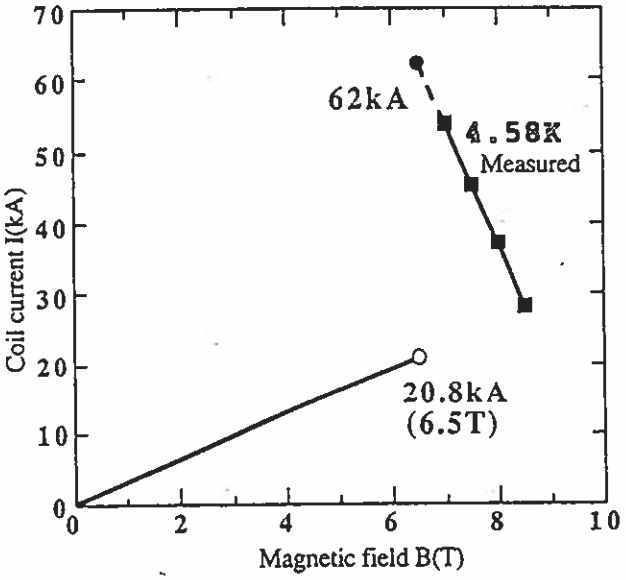

Fig. 4 Design characteristics of the IV coils

V. SUPERCONDUCTING HELICAL COILS

A. General

The design of the helical coils is now being carried out. The winding machine for helical coils is under construction. The helical coil windings will begin in 1994 and be finished in 1997.

Figure 5 shows the cross section of one of the two helical coils. The helical coil winding inside a coil vessel consists of three superconducting blocks, H1-I, H1-M and H1-O. They

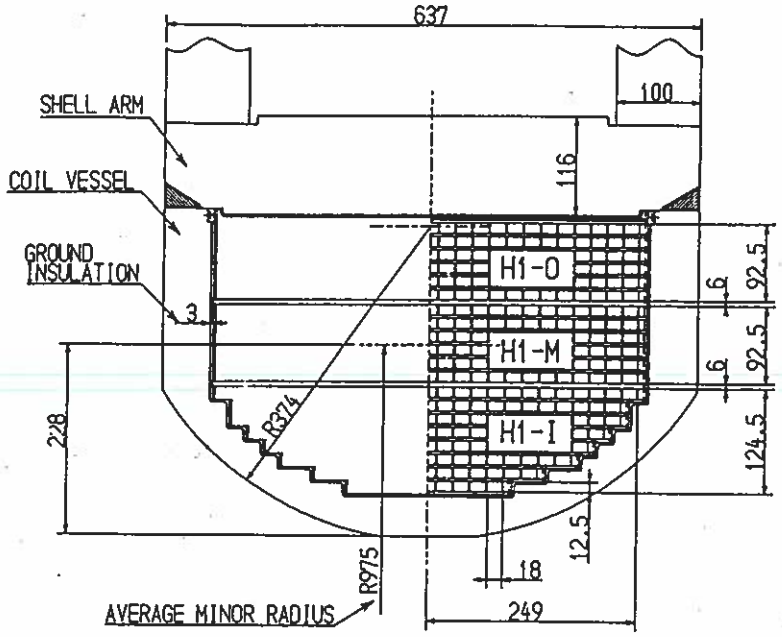

Fig. 5 Cross section of one helical coil

are energized by using three different power supplies in order to change the plasma aspect ratio. Two kinds of thermal shields are set up between the helical coil and the plasma vacuum vessel.

The investigations of the rated current, the size and configuration of the superconductor, and the number of turns of the helical coil were carried out from the viewpoint of stability, coil protection, winding techniques, and heat leak. The rated currents of the helical coils are 13.0 and 17.3 kA in Phase I and Phase II , respectively. Each block has 150 turns. The total number of turns in one helical coil is 450.

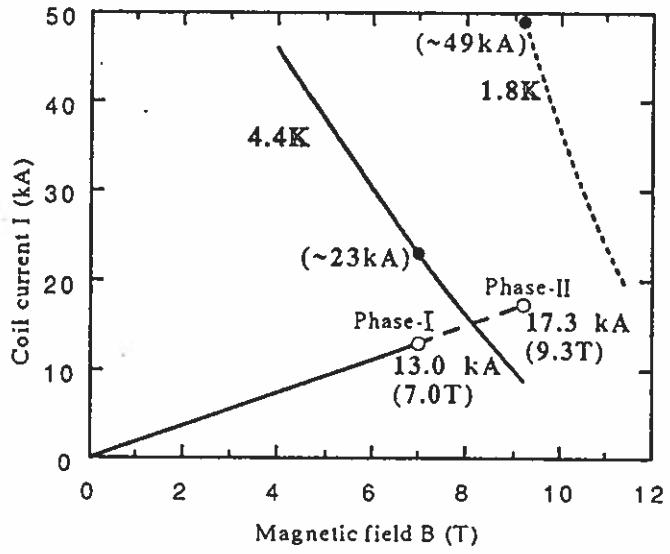

Fig. 6 Design characteristics of the helical coils

B. Superconductor and Coil Winding

The size of the superconductor is planned to be 12.5 by 18.0 mm. It is a composite of Nb-Ti/Cu monoliths and Cu-Al stabilizers. The selection study of superconductor for the helical coils is now ongoing taking into consideration theoretical studies and experiments on critical current, stability, and mechanical stiffness.

The helical coil winding is layer-wound flatwise. There are no superconductor joints within a layer to avoid error fields. Turn-to-turn spacers and layer-to-layer spacers have thicknesses of 2 and 3.5 mm, respectively. The cooling surface ratios between turns and between layers are the same, 67%, at maximum magnetic field region. At lowest and intermediate field regions the cooling surface ratios are reduced to 38 and 50%, respectively. As a result of magnetic force calculations, the maximum compressed pressure of about 100 MPa acts on a spacer, and enhancement of stability of the helical coil is expected.

The design characteristics of the helical coils are shown in Fig. 6. The design fields of 7.0 and 9.3 T are used in Phase I and Phase II, respectively. The design temperature of liquid helium is 4.4 K. The critical current - operating current ratio (I_C/I_{OP}) is designed so as to be 1.7 to 2 based on a permissible disturbance stability theory [5], so that one-layer strand cable can be adopted within the composite conductor for the helical coils.

VI. SUMMARY

The recent status of the design of the superconducting magnets for the Large Helical Device was described. Manufacture of the cryostat, two inner vertical coils, and the helical-coil winding machine are now being carried out. Designs for constructing two helical coils and two other pairs of poloidal coils are being carried on in summer 1992.

REFERENCES

[1] O.Motojima, et al.,"Engineering design study of superconducting Large Helical Device", Plasma Physics and Controlled Nuclear Fusion Research, IAEA-CN-53 /G-1-5 (1990)

[2] J. Yamamoto, O. Motojima, T. Satow, T. Mito and LHD Design Group, "Superconducting Coil Design for Large Helical Device ", IEEE Transactions on Magnetics, Vol.27, No.2 (March 1991) 2220-2223

[3] T, Satow, " Optimum Conditions of Stabilizer Ratio and Critical Current Margin for Maximizing the Current Density of a Tight-wound Superconducting Magnet ", ASC-92, Chicago, LLC-5 (August 1992)

[4] K, Takahata, et al,"Stability of Cable-in-conduit Superconductors for LHD Poloidal Coils",ASC-92, Chicago, LLB-8 (August 1992)

[5] T, Satow, " Steady Cryostatic Stability Criteria of a Quasi- and a Pseudo- Stabilized Superconducting Magnet"(in Japanese), 47th Japanese Cryogenics and Superconductivity Conference, B2-8 (May 1992) 146

LOSSES IN CABLE-IN-CONDUIT SUPERCONDUCTORS USED FOR THE POLOIDAL COIL SYSTEM OF THE LARGE HELICAL DEVICE

F. Sumiyoshi, S. Kawabata, Y. Kanai, T. Kawashima*, T. Mito**, K. Takahata** and J. Yamamoto**
Faculty of Engineering, Kagoshima University, Kagoshima 890,
*Fukuoka Institute of Technology, Fukuoka 811-02,
**National Institute for Fusion Science, Nagoya 464-01, Japan.

Abstract--A NbTi cable-in-conduit conductor encased in a stainless steel jacket is used for the poloidal coil system of the Large Helical Device. This conductor is required to be of high stability, so that it is not allowed to insulate the strands in it and to use CuNi matrix for them in the conductor design. As a result, the inter-strand coupling losses tend to increase during the pulsive operation of the poloidal coil. We measured the loss-frequency characteristics of the short sample conductors with various types of strands in order to clarify their loss properties. The measurement was carried out in the transverse ac ripple field superposed on bias fields, in the frequency range from 0.1 Hz to 200 Hz. Our measuring shows that the replacement of the CuNi-matrix strands in the conductor by the Cu-matrix strands does not much increase the intrinsic coupling loss, but that non-insulation of the strands causes considerably high inter-strand coupling losses.

I. INTRODUCTION

The large helical device (LHD) as an experimental device for fusion science is now under construction at Toki city in Japan[1]. LHD has two large superconducting coil systems, i.e. a helical coil system to provide a confinement field for the hot ionized plasma, and a poloidal coil system to provide the field change. The former coil is projected to be wound by an aluminum stabilized NbTi conductor of pool cooling type, and the latter by a NbTi cable-in-conduit (CIC) conductor of forced-flow cooling type.

The poloidal field coil system is composed of 3 pairs of coils named OV, IS and IV coil. The specification of IV coil, situated at the inmost part of LHD, is as follows: an average radius of 1.8 m, a winding cross section of about $0.47 \times 0.37 m^2$ (2 sets), a maximum overall current density of 29.8 A/mm^2, a maximum magnetic field of 6.5 T and a minimum rising time of 5 seconds. The CIC superconductor for IV coil at operating current of 20.8 kA is required to be of high stability[2,3], so that it is not allowed to insulate the strands. Such a CIC conductor preferentially required to be of high stability tends to generate a large inter-strand coupling loss during the pulsive operation of the coil. The research and development of the CIC conductor is now undergoing from the low loss point of view.

This paper† intends to elucidate the loss feature of the CIC superconductor for the LHD poloidal coil system. Specifically, we shall experimentally show how much the increase in the loss of the high-stability CIC conductor can be. At first we shall describe the characteristics of our experiment for this purpose. Secondly, the results of the loss measurement for several CIC conductors will be shown. Finally, we shall discuss the loss feature of these conductors.

II. EXPERIMENT

A. Sample Preparation

In order to measure the loss property of CIC conductors, we prepared eight conductors as shown in Tab. 1. They are reduced or full scale R&D conductors for the poloidal IV coil of LHD. The parameters of the strands in these conductors are listed in Tab. 2. The conductors differ in the matrix or in the surface condition of the strands.

Only the Conductor TOKI-PF[2] has strands with CuNi and Cu mixed-matrix, while other conductors use strand with Cu matrix. The strands of the Conductors A, TOKI-TF and TOKI-PF, are insulated before assembled. Conductors R-1, R-2, R-3 and IV, are composed of the same type of the strands C-3. They, however, differ in their surface conditions: in the cases of R-2 and R-3, the heat treatment was given for 6 hours and 24 hours at 100 °C in air, respectively, and in other cases, no special treatment was given except the natural oxidation in air.

Short and straight samples of about 500 mm in length are provided for this experiment since bending may change the inter-strand contact condition. As any direct contact of superconducting filaments generates a measurement error of losses, both ends of each short sample are polished to be smooth and flat. A loosely wound single-layered solenoidal-coil of the strand C-3 is also provided for measuring the intrinsic loss in the strand. The diameter and the axis length of the coil are 23.4 mm and 21 mm, respectively.

B. Loss Measurement System

We contrive two kinds of loss measurement systems. The first one is a compact system to measure ac losses in the short and straight sample conductor with a maximum size of 30 mm × 30 mm × 550 mm (in this space for the conductor, the pick-up coil described below must be also mounted together with the sample). In this system, an ac ripple field superposed on a bias one is applied transversely to the long axis of the samples. This is characteristic of our measurement system to carry out this research. The other, an additional system, has a high sensitivity to measure ac losses in the single-strand solenoidal coil sample such as the coil wound by the strand C-3. The coil can be subjected to the ac field with a maximum amplitude of 1 T. In these systems, ac loss measurements are available for a wide frequency range of 0.1-200 Hz. Samples are immersed inliquid helium during the measurement.

In the former system, a saddle-shaped pick-up coil is applied to measure the time variation of the flux inside the short

† The authors are thankful to Mr. H. Takano of Toshiba Corporation for providing samples. This research is supported in part by the Grant in Aid for Scientific Research of the Education Ministry of Japan.
Manuscript received August 24, 1992.

Table 1. Parameters of the sample conductor

Conductor		A	B	TOKI-TF	TOKI-PF	R-1	R-2	R-3	IV
size [mm]		ϕ16.73	ϕ15.20	11×11	17×22.34	ϕ8.15	ϕ8.15	ϕ8.15	22.9×27.7
conduit thickness [mm]		1.05	1.10	1.04	1.0	1.08	1.08	1.08	2.9
void fraction [%]		39.2	36.5	38.3	39.9	38.1	38.1	38.1	38
number of strands		162	162	324	486	36	36	36	486
strand type		C-1	C-1	C-2	CN-1	C-3	C-3	C-3	C-3
insulation of strands		formal	–	formal	formal	–	oxide*	oxide**	–
strand diameter [mm] (after insulation)		0.891	–	0.430	0.67	–	–	–	–
twist pitch [mm]	-3 strands	70	70	35.8	55	61	61	61	60
	-3^2	157	157	67	105	112	112	112	95
	$-3^2\times4$					190	190	190	
	-3^3	245	245	105	164				145
	$-3^3\times6$	500	500						
	-3^4			134	210				225
	$-3^4\times4$			371					
	$-3^4\times6$				580				408

*100°C × 6h, **100°C × 24h (heat treatment in air)

sample. For the sample with a rectangular cross section, the pick-up coil of a few 10 turns of the Cu fine wire is wound encircling the surface of the sample along the axial direction (we call this coil 'pick-up-1'. Cf. Figs. 1 and 3). For the sample with a circular cross section, two kinds of pick-up coils are used: one, named 'pick-up-2', is wound, concentrated parallel to the axis on the circular surface of the sample, and the other, named 'pick-up-3', is wound circumscribing the circular conductor (Cf. Figs. 2 and 4). The absolute value of the loss measured by using pick-up-2 or pick-up-3 is not accurate, but the measured loss-frequency characteristic is reliable.

C. Measured Loss-Frequency Characteristics

Measured loss-frequency characteristic curves are shown in Figs. 1- 4. The vertical axis of these figures, i.e. the 'normalized loss' is the loss per cycle normalized by B_m^2/μ_0, where B_m is the amplitude of the applied ac field, and μ_0 is the permeability of vacuum. Most of the data of the normalized loss do not depend on B_m, which indicates that the measured loss is mainly composed of the joule losses in the normal metal such as the coupling loss or the eddy current loss. The data are, therefore, plotted for the case of B_m=16 Gauss except for the loss of the strand C-3. As for the strand C-3, loss-frequency characteristics were measured for the case of <30 Gauss of which the joule loss predominates over the hysteresis loss in the NbTi filaments.

Table 2. Parameters of the strand in sample conductors

Strand type	C-1	C-2	CN-1	C-3
diameter (bare) [mm]	0.809	0.408	0.65	0.767
Cu/CuNi/SC ratio	3.29/0/1	4.82/0/1	0.4/1.65/1	2.66/0/1
filament diameter[μm]	53	14.1	10.9	15
number of filaments	54	144	1170	690
twist pitch [mm]	28	15	13	9.3
critical current [A]	418 at 3T	37 at 5T	15.2 at 6T	158 at 6.5T

III. RESULTS AND DISCUSSION

A. Losses of the CIC Conductor with Mixed-Matrix Strands

Figure 1 shows the comparison of the losses in two Conductors, TOKI-TF and TOKI-PF, which differ in the matrix of the strands. Both types of the strands, C-2 and CN-1, have a similar structure in which Cu core (we will hereafter denote 'region 3') is at the center of the strand and Cu sheath ('region 1') is outside the filamentary region ('region 2'). But, in the case of the strand of TOKI-PF, CN-1, the filaments surrounded by a small amount of Cu are embedded in CuNi matrix, while in the case of the strand of TOKI-TF, C-2, the filaments are embedded in Cu matrix.

A coupling time constant τ_s^T can be calculated for the strands, CN-1 and C-2, by [4]

$$\tau_s^T = \tau_{s1} + \tau_{s2} + \tau_{s3};$$

$$\tau_{s1} = \frac{1}{2}\sigma_{Cu}\mu_0\left(\frac{L_s}{2\pi}\right)^2\left(\frac{R_2}{R_1}\right)^2\frac{R_1^2-R_2^2}{R_1^2+R_2^2},$$

$$\tau_{s2} = \frac{1}{2}\sigma_2\mu_2\left(\frac{L_s}{2\pi}\right)^2\frac{R_2^2-R_3^2}{R_1^2},$$

$$\tau_{s3} = \frac{1}{2}\sigma_{Cu}\mu_0\left(\frac{L_s}{2\pi}\right)^2\left(\frac{R_3}{R_1}\right)^2, \qquad (1)$$

where the suffix, 1, 2 or 3, corresponds to each region, τ_{s1}, τ_{s2} or τ_{s3} is the contribution to the overall coupling time constant,

σ_{Cu} is the conductivity of Cu (~1×10^{10} S/m at 0~0.9T), Ls is the twist pitch of the strands, and R_1, R_2 and R_3 is the outer radius of each region. The conductivity of the region 2, σ_2, is denoted by [5]

$$\sigma_2 = \sigma_{CuNi}\frac{1+\lambda_2'}{1-\lambda_2'} \quad \text{for Strand CN-1,} \tag{2}$$

$$\sigma_2 \sim \sigma_{Cu} \quad \text{for Strand C-2,} \tag{3}$$

where σ_{CuNi} is the conductivity of CuNi, and λ_2' is the volume fraction of the filaments and Cu in the region 2. The permeability of the region 2, μ_2 is given as $\mu_2 = \mu_0(1-\lambda_2)/(1+\lambda_2)$ for the small field case, where λ_2 is the volume fraction of the filaments in the region 2. On the other hand, the frequency characteristics of the normalized coupling current loss in the strands, w_s, is given by

$$w_s = 2\,w_p\frac{f/f_s}{1+(f/f_s)^2}. \tag{4}$$

In this equation, $f_s(\equiv 1/(2\pi\tau_s))$ is the coupling peak frequency of the strands, and w_p is the peak value of w_s, i.e.

$$w_p = \pi\frac{\mu_{eff}}{\mu_0}\ ;\ \mu_{eff}\sim\mu_0\frac{1-\lambda_{tot}}{1+\lambda_{tot}}, \tag{5}$$

where λ_{tot} is the volume fraction of the filaments in the whole strand.

Table 3 shows the results of the loss properties of different strands in some conductors. The superscripts 'T' and 'E' represent the theoretical and the experimental results respectively. From this table, we can see that there is not much difference in τ_s^T between C-2 and CN-1. The measured results shown in Fig. 1 and Tab. 3 support this theoretical prediction. The strand with a mixed-matrix, dealt with in this paper, is not a popular strand, but only an example for trial. This result suggests, however, that the strands with Cu matrix for high stability do not have significantly larger coupling losses.

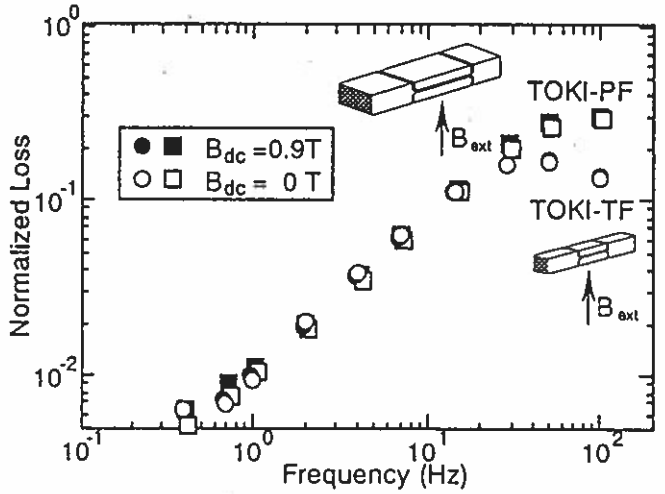

Fig. 1 Measured frequency characteristics of the normalized losses in the Conductors TOKI-TF and TOKI-PF.

B. Losses of the CIC Conductor with Non-Insulated Strands

Figures 2 and 3 show the observed loss-frequency characteristics of the Conductors with non-insulated strands. As shown in Fig. 2, the difference in characteristics among the three Conductors, R-1, R-2 and R-3, is not so considerable, which indicates that the heat treatment of R-2 and R-3 in air for changing their surface conditions does not play an important role to reduce losses. On the other hand, the observed loss-frequency characteristic of the Conductor IV, as shown in Fig.3, is very different from that shown in Fig. 2.

We will now discuss what these characteristics indicate. The dotted lines in Fig. 2 and Fig. 3 represent the loss-frequency characteristics measured for the single-layered solenoidal-coil of the strand C-3. The absolute value of the normalized loss is adjusted as follows: the loss of the Conductors R-1 and IV is assumed to be equal to w_s+w_c, where w_s is the measured loss of the strand C-3 multiplied by a constant α, and the inter-strand coupling loss w_c is given as

$$w_c = 2\,\beta\frac{f/f_c}{1+(f/f_c)^2}. \tag{6}$$

In this equation, β is the peak value of w_c, which is a constant, and f_c is the frequency corresponding to β. These three values, α, β and f_c, are adjustable parameters, which are determined by fitting our theoretical formulae to the observed data of the Conductors. From the obtained results, which are shown as w_s and w_c in Figs. 2 and 3, we notice that the loss value w_c of the Conductor IV is higher than that of the Conductor R-1. This result seems to be reasonable on account of the difference in both the maximum twist pitch of cabling and the number of cabling stages. A quantitative explanation is, however, required to design the final CIC conductor for the poloidal IV coil of LHD.

Table 3. Results on loss properties of various strands

Strand	C-1	C-2	CN-1	C-3
Sample conductor	A	TOKI-TF	TOKI-PF	(Solenoid)
Theoretical results				
-Coupling time constant of strands, τ_s^T [msec]	78	15.4	7.4	4.9
-Coupling peak frequency of strands, $f_s^T \equiv 1/(2\pi\,\tau_s^T)$ [Hz]	2.0	10.3	22	32
-Peak value of normalized coupling losses in samples, w_p^T	0.75	0.78	0.67	1.8
Experimental results				
-Peak frequency, $f_s^E \equiv 1/(2\pi\,\tau_s^E)$ [Hz]	2.7	43	75	20
-Peak loss value, w_p^E	0.14	0.18	0.30	0.60
Comparison				
$-\tau_s^E/\tau_s^T$	0.74	0.24	0.29	1.6
$-w_p^E/w_p^T$	0.19	0.23	0.45	0.33

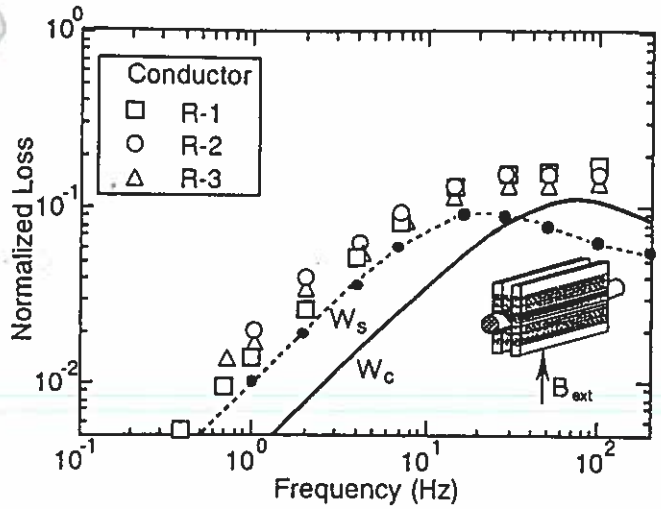

Fig. 2 Measured frequency characteristics of the normalized losses in the Conductors, R-1, R-2 and R-3, where Bdc = 0T. A dotted line with dark circles corresponds to the strand C-3. A solid line corresponds to the estimated inter-strand coupling loss in the Conductor R-1.

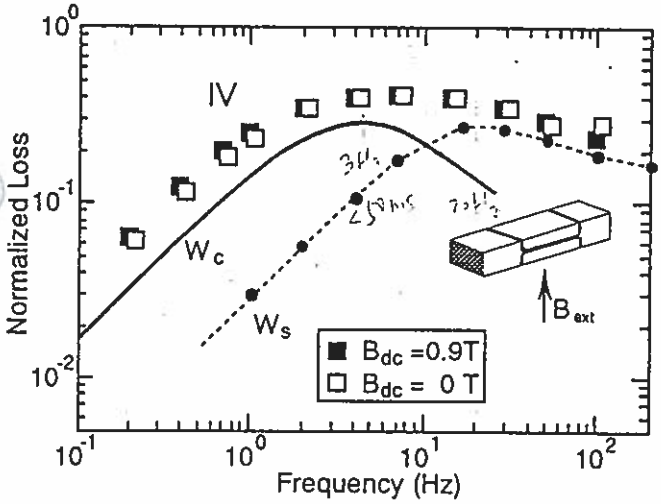

Fig. 3 Measured frequency characteristics of the normalized losses in the Conductor IV. A dotted line with dark circles corresponds to the strand C-3. A solid line corresponds to the estimated inter-strand coupling loss.

IV. CONCLUSION

We measured the loss-frequency characteristics of the high-stability NbTi CIC conductors in order to clarify the loss feature of the conductor for the LHD poloidal coil. The conductor required to be of high stability is not allowed to insulate strands in it and to use CuNi matrix for them in the conductor design. Our measurements for such conductors show that the exchange of the CuNi-matrix strands in it for the Cu-matrix strands does not much increase the intrinsic coupling loss, but that non-insulation of strands causes considerably high inter-strand coupling losses.

REFERENCES

[1] O. Motojima and LHD Design Group, "Design status of superconducting large helical device," IEEE Trans. Magn., vol. 27, pp. 2214-2219, March 1991.

[2] J. Yamamoto, K. Takahata, T. Mito, N. Yanagi, S. Yamada, A. Nishimura, M. Sakamoto, O. Motojima and M. Fujiwara, "Forced-cooled Nb-Ti poloidal test coil for large helical device," Cryogenics, vol.. 32, pp. 445-448, May 1992.

[3] K. Takahata, T. Mito, N. Yanagi, M. Sakamoto, S. Yamada, A. Nishimura, J. Yamamoto, S. Mizukami, K. Nakamoto, T. Uchida, Y. Wachi, M. Shimada, S. Itoh and S. Ioka, "Stability of cable-in-conduit superconductors for LHD poloidal coils," Presented at Appl. Super. Conf. (LLB-8), Chicago, Illinois, August 1992.

[4] B. Turck, "Coupling losses in various outer normal layers surrounding the filament bundle of a superconducting composite," J. Appl. Phys., vol. 50, pp. 5397-5401, August 1979.

[5] F. Sumiyoshi, F. Irie and K. Yoshida, "The effect of demagnetization on the eddy-current loss in a single-layered multifilamentary superconducting coil," J. Appl. Phys., vol. 51, pp. 3807-3811, July 1980.

APPENDIX

An additional measurement is carried out concerning the increase in the inter-strand coupling loss in the case of non-insulated strands. Figure 4 shows the difference in the loss-frequency characteristic curves between the Conductor A and B. These conductors are composed of the strands designed for MRI. The curve of the Conductor A is just the same as the Debye curve predicted theoretically, and that of the Conductor B is similar to that of the Conductors, R-1, R-2 and R-3, shown in Fig. 2 except that f_s is smaller by about 1 order.

Unfortunately, the pick-up coils are the type of the pick-up-2. In addition, the size of the two coils of the Conductors A and B is different each other, so that the difference between the two curves of their coupling current loss is due to non-insulation around the strands. According to the argument similar to the one in the case of Figs. 2 and 3, f_c is much higher than f_s. It means that the inter-strand coupling loss dose not predominate over the intrinsic coupling loss in the strand.

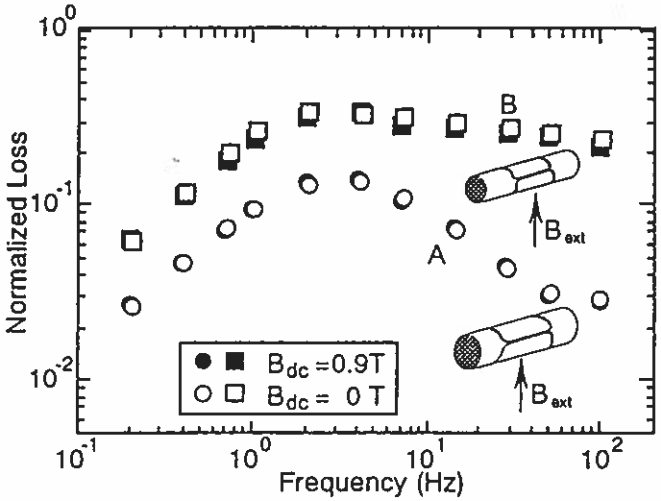

Fig. 4 Measured frequency characteristics of the normalized losses in the Conductors A and B.